nagra National Cooperative for the Disposal of Radioactive Waste

TECHNICAL REPORT 95-01

Heterogeneous Redox Reactions in Groundwater Flow Systems - Investigation and Application of Two Different Coupled Codes

May 1995

W. Pfingsten
C.L. Carnahan

PSI, Würenlingen and Villigen

Hardstrasse 73, CH-5430 Wettingen/Switzerland, Telephone +41-56-37 11 11

nagra National Cooperative for the Disposal of Radioactive Waste

TECHNICAL REPORT 95-01

Heterogeneous Redox Reactions in Groundwater Flow Systems - Investigation and Application of Two Different Coupled Codes

May 1995

W. Pfingsten
C.L. Carnahan*

PSI, Würenlingen and Villigen

* Present address:

14 Camino Sobrante;
Orinda, California 94563 (USA)

Hardstrasse 73, CH-5430 Wettingen/Switzerland, Telephone +41-56-37 11 11

This report was prepared on behalf of Nagra. The viewpoints presented and conclusions reached are those of the author(s) and do not necessarily represent those of Nagra.

Abstract

Two simulators of reactive chemical transport are applied to a set of problems involving heterogeneous redox reactions of uranium species. The simulators use similar algorithms to compute the heterogeneous chemical equilibria, but they use distinctly different approaches to the computation of solute transport and to the coupling of transport with chemical reactions. One simulator (MCOTAC) sequentially couples calculations of static chemical equilibria to a random-walk simulation of solute advection and dispersion. The other simulator (THCC) directly couples mass action relations for chemical equilibria to finite-difference representations of the solute transport equations.

The aim of the comparison was to demonstrate the applicability of the newly developed code MCOTAC to redox problems, and to identify and investigate general differences between the two types of codes within these applications. The chosen heterogeneous redox systems are hypothetically generated systems which provide numerical difficulties within the coupled code calculation. Uranium, an important component of heterogeneous redox systems consisting of uraniferous solids and natural groundwaters, was chosen as a main component in the example redox systems because of practical interest for performance assessment of geological repositories for nuclear wastes.

The calculations show reasonable agreement, in general, between the two computational approaches. Specific areas of disagreement arise from numerical difficulties peculiar to each approach. Such "benchmarking" can enhance confidence in the overall performance of individual simulators while identifying aspects that may require further investigations and possible modifications.

Zusammenfassung

Zwei numerische Modelle, die den chemisch-reaktiven Transport beschreiben, werden auf einen Satz von Problemen angewendet, die heterogene Redoxreaktionen von Uranspezies enthalten. Die Modelle verwenden ähnliche Algorithmen zur Berechnung der heterogenen chemischen Gleichgewichte, aber sie verwenden eine deutlich unterschiedliche Beschreibung des Transports und der Kopplung zwischen Transport und chemischen Gleichgewichtsreaktionen. Im Code MCOTAC sind statisches chemisches Gleichgewicht und eine Random-Walk Beschreibung von Advektion und Dispersion für wasserlösliche Substanzen sequentiell miteinander gekoppelt. Im Code THCC sind die Massenwirkungsgesetze der Gleichgewichtschemie mit einer finiten Differenzen Beschreibung der Transportgleichungen für wasserlösliche Substanzen direkt miteinander gekoppelt.

Ziel dieses Vergleichs war es, die Anwendung des neu entwickelten Rechenprogramms MCOTAC auf Redox-Probleme anzuwenden und, innerhalb dieser Anwendungen, generelle Unterschiede zwischen den zwei Typen von Rechenprogrammen zu identifizieren und zu untersuchen. Die hypothetischen heterogenen Redox-Systeme sind dabei so ausgewählt, das sie numerische Schwierigkeiten innerhalb der gekoppelten Berechnungen garantieren. Uran, eine Hauptkomponente der Beispiel-Redox-Systeme, ist ein chemisch interessantes Element für heterogene Redox-Systeme, die Uran-Eisen-Mineralien und Komplexe mit Liganden beinhalten. Diese kommen in natürlichen Grundwässern vor und sind von praktischem Interesse bei Sicherheitsanalysen von geologischen Endlagern für radioaktive Abfälle.

Die Berechnungen der beiden Programme zeigen i.A. eine gute Übereinstimmung der Ergebnisse. Spezifische Diskrepanzen ergeben sich bei numerischen Schwierigkeiten der Codes und sind unterschiedlich für jeden Code. Ein derartiges "Benchmarking" kann das Vertrauen in der allgemeinen Anwendbarkeit von einzelnen Programmen verbessern, indem programmspezifische Aspekte aufgezeigt werden, die weitere Untersuchungen und mögliche Modifikationen erfordern.

Résumé

Deux modèles numériques de transport et réactions chimiques sont appliqués à un ensemble de problèmes liés aux réactions redox hétérogènes de l'espèce Uranium. Les deux modèles utilisent des algorithmes semblables en ce qui concerne la modélisation des équilibres chimiques hétérogènes mais utilisent des approches différentes en ce qui concerne la modélisation du transport du soluté et du couplage du transport avec les réactions chimiques. Un premier modèle (MCOTAC) couple séquentiellement le calcul des équilibres chimiques statiques avec une simulation de marche au hasard pour l'advection et la dispersion du soluté. L'autre modèle (THCC) couple directement les lois d'action de masse pour les équilibres chimiques avec des représentations en différences finies pour les équations du transport du soluté.

Le but de cette comparaison était de démontrer l'applicabilité du code nouvellement développé MCOTAC aux problèmes de redox, et d'identifier et d'étudier les différences générales entre les deux types de modèles, dans le cadre de ces applications. Les systèmes redox hétérogènes choisis sont des systèmes générés hypothétiquement et qui posent des difficultés numériques lors de la résolution du modèle couplé. L'Uranium, un composant important des systèmes redox hétérogènes constitués par des minéraux uranifères et des eaux souterraines naturelles, a été choisi comme composant principal dans l'exemple des systèmes redox à cause de son intérêt pratique dans l'estimation des risques dûs au stockage géologique des déchets nucléaires.

Les calculs montrent, en général, un accord satisfaisant entre les deux approches numériques. Des zones spécifiques de désaccord surgissent à cause des difficultés numériques propres à chaque approche. Un tel "benchmark" peut augmenter la confiance dans la performance globale de chaque modèle et en même temps identifier des aspects qui devraient requérir des études ultérieures et des modifications possibles.

Contents

List of figures

List of tables

List of symbols

D	dispersivity
$E°$	standard electrode potential
Eh	oxidation potential
F	Faraday constant
$K(T)$	equilibrium constant of a reaction at temperature T
K_f	equilibrium constant used for formation of complexes
K_{sp}	equilibrium constant used for formation or dissolution of solids (solubility product)
n	number of electrons e^- transferred
Pe	Peclet number
R	gas constant
t	time
T	absolute temperature in Kelvins
v	flow velocity
x	spatial coordinate
γ_s	activity coefficient
ΔG_r^0	standard free energy of reaction
ΔG_f^0	standard free energy of formation
Δx	spatial grid size
[s]	activity of solute s
(s), s	concentration of solute s

1. Introduction

Although most redox reactions are kinetically controlled, equilibrium considerations can help to understand redox systems in a general way. Equilibrium calculations provide boundary conditions toward which the system must proceed [Stumm & Morgan, 1981]. Further difficulties occur in respect to available data for a kinetic description. In principle, redox reactions are not a new type of reaction for a chemical equilibrium model which includes formation of complexes and dissolution/precipitation reaction. To simulate such reactions during flow of groundwater, a chemical equilibrium model is coupled to a solute transport or fluid-flow model. Two different coupled codes were applied to heterogeneous redox problems in groundwater flow systems: a directly coupled code THCC and a sequentially coupled code MCOTAC which are explained in detail in [Carnahan, 1986] and [Pfingsten, 1994].

Within the directly coupled code the advective-dispersive transport equations, described by a finite difference formulation, and the set of chemical equilibrium equations are solved in one step, whereas the sequentially coupled code solves the chemical equilibrium equations and the transport equations separately. The last code uses for the advective-dispersive transport descriptions a multi-species random walk method in contrast to the directly coupled code. The calculation of chemical equilibria is in both codes very similar.

The aim of the comparison of the two code applications was to demonstrate the applicability of the newly developed code MCOTAC to redox problems in comparison to the directly coupled code applications, and to identify and investigate general differences between the two types of codes within these applications. The chosen heterogeneous redox systems are hypothetically generated systems that guarantee numerical difficulties within the coupled code calculation. A successful handling of these systems by the codes then should allow a handling of simpler problems.

Uranium was chosen as a main component in the example redox systems. Uranium is chemically interesting because of its possible existence in four oxidation states (III, IV, V, VI), its ability to form complexes with ligands occurring in natural waters, and the existence of heterogeneous redox equilibria involving uraniferous solids. Further, uranium is of practical interest for investigations of formation of ore bodies and for performance assessment of geological repositories for nuclear wastes [Carnahan, 1988].

First, the handling of redox problems within the codes is defined for understanding. This includes a description of the physico-chemical systems to be modelled and the extraction of thermodynamically relevant data out of the used data base. Then a comparison of calculations of the two coupled codes is presented. Concentration profiles of chemical species calculated by the two codes are compared, as well as the used computation time. Individual problems or features of the two codes are discussed and compared within the different example redox systems. The investigations include a comparison of the different descriptions of the transport within the codes, the advantages or disadvantages of the codes within these applications, and general problems during application of coupled codes, e.g., the definition of the system in terms of chosen grid size or chosen set of basis species for the dynamical equilibrium calculations. The comparison of the codes also may assist in deciding

which code should be applied to a given problem, depending on the experiences gained from code applications on example problems.

2. General chemical relations and examples for redox systems

Consider a general redox couple, *"ox-red"*, in which the members *"ox"* and *"red"* are different oxidation states of the same chemical element, *"ox"* representing the higher state and *"red"* the lower state. The reaction for the reduction of *"ox"* to *"red"* with transfer of n electrons e^- can be written very generally as

$$ox + ne^- = red \tag{2-1}$$

where ionic charges and other possible reactants and products have been omitted for clarity. The standard electrode potential, $E°$, of the reaction as written in (2-1) is given by:

$$E° = \frac{RT}{nF} \ln K(T) \tag{2-2}$$

where R is the universal gas constant, 8.3145 J/(mol K), T is the absolute temperature in Kelvins (K), F is the Faraday constant, 96485 C/mol, and $K(T)$ is the equilibrium constant for the reaction at temperature T. The oxidation potential, Eh, of a system containing the couple *"ox-red"* is given by:

$$Eh = E° + \frac{RT}{nF} \ln \frac{[ox]}{[red]} \tag{2-3}$$

where [...] denote activities of the members of the couple under current system conditions. Note that the activity of a solute "s" is the product of its concentration and an activity coefficient, γ_s, thus $[s] = \gamma_s$ (s), where the notation (...) is used here to represent the concentration. Activity and concentration bear the same units, mol/dm³, M. At the temperature 298.15 K, the quantity $RT/F = 0.025693$ V, and $(RT/F)ln10 = 0.05916$ V. Both $E°$ and Eh are referenced to $E° = 0$ for the standard hydrogen electrode. The equilibrium constant, $K(T)$, of a chemical reaction is calculated from the thermodynamic relation:

$$\ln K(T) = -\frac{\Delta G_r^0}{RT} \tag{2-4}$$

where ΔG_r^0 is the standard free energy of reaction at T. ΔG_r^0 is found by algebraically summing up the weighted standard free energies of formation at T, ΔG_f^0, of reactants and products. The weights are stoichiometric coefficients for the reaction.

The conventions used in the computer programs THCC and MCOTAC are illustrated by the following examples.

a) For the reduction of Fe^{3+} to Fe^{2+},

$$Fe^{3+} + e^- = Fe^{2+} \tag{2-5}$$

the ΔG_f^0 values for Fe^{3+}, e^-, and Fe^{2+} are respectively, -17.238, 0., and -91.504 kJ/mol[1]. Then ΔG_r^0 = -74.266 kJ/mol, $log\ K = 13.0108$, and E° = 0.7697 V. The *Eh* (in V) of a system containing this couple is given by:

$$Eh = 0.7697 + 0.05916 \log \frac{[Fe^{3+}]}{[Fe^{2+}]} \tag{2-6}$$

b) For the reduction of H^+ to H_2(aq),

$$2H^+ + 2e^- = H_2(aq) \tag{2-7}$$

the ΔG_f^0 values for H^+, e^-, and H_2(aq) are respectively, 0., 0., and 17.723 kJ/mol. Then ΔG_r^0 = 17.723 kJ/mol, $logK$ = -3.1049, and E° = -0.0918 V. The *Eh* of a system containing this couple is given by:

$$Eh = -0.0918 + 0.02958 \log \frac{[H^+]^2}{[H_2(aq)]} \tag{2-8}$$

or

$$Eh = -0.0918 - 0.05916\, pH - 0.02958 \log[H_2(aq)] \tag{2-9}$$

c) For the reduction of UO_2^{2+} to $U(OH)_4(aq)$,

$$UO_2^{2+} + 2e^- + 2H_2O(l) = U(OH)_4(aq) \tag{2-10}$$

the ΔG_f^0 values for UO_2^{2+}, e^- H_2O(l), and $U(OH)_4$(aq) are respectively, -952.556, 0., -237.183, and -1452.600 kJ/mol. Then ΔG_r^0 = -25.678 kJ/mol, $logK = 4.4985$, and E° =0.1331 V. The *Eh* of a system containing this couple is given by:

$$Eh = 0.1331 + 0.02958 \log \frac{[UO_2^{2+}]}{[U(OH)_4(aq)]} \tag{2-11}$$

---

[1]The data used to describe the chemical equilibrium (equilibrium constants or *logK* values) were extracted from the EQ3/6 data base (EQ3/6 data base DATA0COM.R14 (June 1992) used at Lawrence Berkeley Laboratory), there written as Gibbs free energies of formation. The data transformation from Gibbs free energies of formation to equilibrium constants, used here, is responsible for the "apparent" accuracy of the given *logK* values within the redox examples. The "apparent" accuracy is not related to experimentally available data, but it was necessary to assure a consistent application and comparison of the two coupled codes.

Note that H_2O(l) must be included in the calculation of ΔG_f^0 but it is omitted from the formulation of *Eh* because in the latter case the activity coefficient of H_2O(l) is assumed to be unity always.

In the computer programs THCC and MCOTAC the equilibrium constants used for complexes are *formation constants*, K_f, and those used for solids (minerals) are *solubility products*, K_{sp}. The formation of a complex without redox, using UO_2^{2+} as a basis species, is exemplified by UO_2OH^+:

$$UO_2^{2+} + H_2O(l) - H^+ = UO_2OH^+ \qquad (2\text{-}12)$$

Using ΔG_f^0 values stated previously and -1160.010 kJ/mol for UO_2OH^+, $\Delta G_r^0 = 29.729$ kJ/mol and $K_f = 6.19 \cdot 10^{-6}$. For formation of the complex $U(OH)_4$(aq) through reduction of UO_2^{2+} by Fe^{2+},

$$UO_2^{2+} + 2Fe^{2+} + 2H_2O(l) - 2Fe^{3+} = U(OH)_4(aq) \qquad (2\text{-}13)$$

$\Delta G_r^0 = 122.854$ kJ/mol and $K_f = 3.00 \cdot 10^{-22}$.

Dissolution of a solid without redox is exemplified by schoepite:

$$UO_2(OH)_2 \cdot H_2O(s) = UO_2^{2+} + 3H_2O(l) - 2H^+ \qquad (2\text{-}14)$$

Using ΔG_f^0 values stated previously and -1636.516 kJ/mol for $UO_2(OH)_2 \cdot H_2O(s)$, ΔG_r^0 = -27.589 kJ/mol and $K_{sp} = 6.81 \cdot 10^4$. The solid uraninite is formed by reduction of UO_2^{2+} by H_2(aq),

$$UO_2(s) = UO_2^{2+} + H_2(aq) - 2H^+ \qquad (2\text{-}15)$$

Using ΔG_f^0 values stated previously and -1031.829 kJ/mol for $UO_2(s)$, $\Delta G_r^0 = 96.996$ kJ/mol and $K_{sp} = 1.02 \cdot 10^{-17}$.

It is noted that the free electron, e^-, (a hypothetical species) appears only in the so-called *half-cell* reactions such as (2-1), (2-5), (2-7) and (2-10). Reactions of this type are used for the so-called indirect method of redox reactions in which e^- appears explicitly as a basis species and plays the role of the *master* reducing species. For the so-called direct method, redox reactions are written as *whole-cell* reactions in which the species e^- does not appear. Instead, a *master redox couple* is specified, and both members of this couple must be designated to be basis species. Other redox couples are included by designating the oxidised member of each couple to be the basis species and the reduced member to be a complex or solid. Then, in the direct method, every redox reaction must contain two couples of which one must be the master redox couple. Such reactions are exemplified here by (2-13), in which the master couple is Fe^{3+}-Fe^{2+}, and by (2-15), in which the master couple is H^+-H_2(aq).

3. Simulation of a uranium-iron redox system

3.1 Definition of the system

Within this system, a solution containing uranium and iron at Eh = -0.1807 V and $pH = 8$ flows into a spatial domain of solution containing iron at Eh = -0.4148 V and $pH = 10$ [2]. Both solutions contain carbonate, as CO_2(aq), HCO_3^- and CO_3^{2-}, at a total aqueous concentration[3] of $3 \cdot 10^{-4}$ M. Basis species are UO_2^{2+}, Fe^{3+}, Fe^{2+}, CO_3^{2-}, H^+, and Na^+. Na^+ serves as a non-reactive tracer of solute transport, and its concentration is determined by charge balancing. H_2O(l) is assumed to be present at constant unit activity and is not included in the species list; H_2O(l) can participate in complex- and solid-forming reactions.

---

[2]These values are the result of the chosen basis species concentrations, the chosen complexes within the modelling, and the equilibria with the solids UO_2(s), and $FeOOH$(s) for the inflowing solution, and with $FeOOH$(s) for the domain solution.

[3]Total concentration of a basis species j, $X_{j,total}$, is equal to the sum over all species concentrations (basis species X_j, N_c complexed species C_i, and N_k solid species P_k) bearing the basis species X_j weighted by the stoichiometric coefficients A_{ij} and B_{jk} [Pfingsten, 1994]:

$$X_{j,total} = X_j + \sum_{i=1}^{N_c} A_{ij} C_i + \sum_{k=1}^{N_k} B_{jk} P_k$$

With this mathematical definition, the value of the total concentration of a basis species can be negative, depending on the chemical system, e.g., if dissociation of water is included in the chemical equilibrium calculation in 4.2.1, it depends on the choice of OH^- or H^+ as a basis species, whether a basis species has positive or negative total concentration (see also footnote 13). In this case the total concentration is an operational total concentration with no direct chemical meaning. Similarly, the total aqueous concentration is defined as the sum over all species in the aqueous phase (basis species X_j and complexed species C_i) bearing the basis species X_j weighted by the stoichiometric coefficients A_{ij}. This sum corresponds to the first two terms of the right side of the equation above.

Table 3.1: Chemical reactions and logK values (at 25° C) used in simulations of uranium-iron systems (see footnote 1)

reaction	*logK*
$H_2O(l) - H^+ = OH^-$	–13.9954
$CO_3^{2-} + H^+ = HCO_3^-$	10.3288
$CO_3^{2-} + 2H^+ - H_2O(l) = CO_2(aq)$	16.6737
$Fe^{3+} - 3H^+ + 3H_2O(l) = Fe(OH)_3(aq)$	–12.1735
$Fe^{3+} - 4H^+ + 4H_2O(l) = Fe(OH)_4^-$	–21.6011
$Fe^{2+} - 2H^+ + 2H_2O(l) = Fe(OH)_2(aq)$	–20.6004
$Fe^{2+} + CO_3^{2-} + H^+ = FeHCO_3^+$	12.3790
$UO_2^{2+} + CO_3^{2-} = UO_2CO_3(aq)$	9.61470
$UO_2^{2+} + 2CO_3^{2-} = UO_2(CO_3)_2^{2-}$	16.9698
$UO_2^{2+} + 3CO_3^{2-} = UO_2(CO_3)_3^{4-}$	21.5845
$UO_2^{2+} - 2Fe^{3+} + 2Fe^{2+}\ 2H_2O(l) = U(OH)_4(aq)$	–21.5230
$UO_2(s) = UO_2^{2+} - 2Fe^{3+} + 2Fe^{2+}$	12.1336
$FeOOH(s) = Fe^{3+} + 2H_2O(l) - 3H^+$	0.53504

Table 3.2: Inlet concentrations of basis species in solution and amounts of solids used to specify the inlet solution. Negative total aqueous concentration is the result of the chosen basis species and has no chemical meaning but it is relevant within the mathematical framework. The solid concentrations are given for completeness to allow comparison to codes using total basis species concentration (see footnotes 1 and 3).

Basis Species	total aqueous concentration [mol/l]	species concentration [mol/l]
UO_2^{2+}	$4.0795 \cdot 10^{-10}$	$1.0879 \cdot 10^{-20}$
Fe^{3+}	$-8.1350 \cdot 10^{-10}$	$4.0754 \cdot 10^{-24}$
Fe^{2+}	$4.5112 \cdot 10^{-8}$	$4.2990 \cdot 10^{-8}$
CO_3^{2-}	$3.0000 \cdot 10^{-4}$	$1.4537 \cdot 10^{-6}$
H^+	$3.0387 \cdot 10^{-4}$	$1.0190 \cdot 10^{-8}$
Na^+	$2.9605 \cdot 10^{-4}$	$2.9605 \cdot 10^{-4}$
UO_2(s)	present at $5.9203 \cdot 10^{-10}$	
$FeOOH$(s)	present at $3.5036 \cdot 10^{-9}$	

Table 3.3: Initial concentrations of basis species in solution and amounts of solids in the model spatial domain (see footnotes 1 and 3).

Basis Species	total aqueous concentration [mol/l]	species concentration [mol/l]
UO_2^{2+}	0.0	0.0
Fe^{3+}	$1.1134 \cdot 10^{-11}$	$4.3783 \cdot 10^{-30}$
Fe^{2+}	$4.9970 \cdot 10^{-10}$	$4.0130 \cdot 10^{-10}$
CO_3^{2-}	$3.0000 \cdot 10^{-4}$	$1.0127 \cdot 10^{-4}$
H^+	$9.4807 \cdot 10^{-5}$	$1.0270 \cdot 10^{-10}$
Na^+	$5.0520 \cdot 10^{-4}$	$5.0520 \cdot 10^{-4}$
UO_2(s)	-	
FeOOH(s)	present at $4.7489 \cdot 10^{-8}$	

The master redox couple is Fe^{3+} - Fe^{2+}. This couple participates in redox reactions forming the aqueous complex $U(OH)_4$(aq) and the solid UO_2(s), by which *U*(VI) is reduced to *U*(IV) and Fe^{2+} is oxidised to Fe^{3+}. *U*(VI) is present in the basis species UO_2^{2+} and its complexes UO_2CO_3(aq), $UO_2(CO_3)_2^{2-}$ and $UO_2(CO_3)_3^{4-}$. Basis species Fe^{3+} forms *Fe*(III) complexes $Fe(OH)_3$(aq) and $Fe(OH)_4^-$ and the solid *FeOOH*(s) (goethite), while basis species Fe^{2+} forms *Fe*(II) complexes $Fe(OH)_2(aq)$ and $FeHCO_3^+$.

The objective of this simulation was to illustrate the reduction of *U*(VI) in the inflowing solution by Fe^{2+} in the spatial domain solution, resulting in precipitation of UO_2(s) within the domain. The inflowing solution was required to be at equilibrium with UO_2(s), and both solutions were required to be at equilibrium with *FeOOH*(s).

As the simulation, in the dynamic mode, progresses through time, UO_2(s) is precipitated near the influx boundary, and the region of precipitation extends progressively further along the domain. No change is observed in the concentration of *FeOOH*(s) in the domain, established by the initial equilibration. In the region of UO_2(s) precipitation, the concentration of $U(OH)_4$(aq) remains constant throughout time and space at $4.079 \cdot 10^{-10}$ M in the inflowing solution. The concentration of $Fe(OH)_3$(aq) is constant in time and space at $2.299 \cdot 10^{-12}$ M due to equilibrium with *FeOOH*(s) established for both, inflowing and domain solutions by the initial conditions. These aspects are discussed in greater detail in the following paragraphs.

Consider the chemical equilibria involved in reduction of *U*(VI) species to *U*(IV) in the form of UO_2(s) and $U(OH)_4$(aq). The computer programs pose these equilibria in terms of the set of basis species which is the minimum set of species to form all complexes and solids. Thus, the dissolution of UO_2(s) is described by an expression for the solubility product with the basis species UO_2^{2+}, Fe^{3+}, *and* Fe^{2+}:

$$UO_2(s) = UO_2^{2+} - 2Fe^{3+} + 2Fe^{2+},\ K_{sp} = 1.360 \cdot 10^{12} \quad (3\text{-}1)$$

The formation of complex $U(OH)_4$(aq) is described by:

$$UO_2^{2+} - 2Fe^{3+} + 2Fe^{2+} + 2H_2O(l) = U(OH)_4(aq),\ K_f = 2.999 \cdot 10^{-22} \quad (3\text{-}2)$$

These expressions can be combined to describe the equilibrium between U(IV) species:

$$UO_2(s) + 2H_2O(l) = U(OH)_4(aq),\ K_{sp}' = [U(OH)_4(aq)] = 4.079 \cdot 10^{-10} \quad (3\text{-}3)$$

It is seen that, in the presence of UO_2(s), the concentration of $U(OH)_4$(aq) (equal to activity because of zero charge) must remain constant at the value $4.079 \cdot 10^{-10}$ M, and this equilibrium is not affected by either *pH* or *Eh*. This means that precipitation of UO_2(s) in the domain is due to reduction of U(VI) and is independent of the *pH* changes. Because the concentration of $U(OH)_4$(aq) cannot rise above the inflowing solution value of $4.079 \cdot 10^{-10}$ M, the "new" U(IV) in excess above this limit must be precipitated as UO_2(s). The limit remains constant regardless of conditions of *Eh* and *pH*.

A similar effect controls the concentration of the aqueous *Fe*(III) species, $Fe(OH)_3$(aq), in the presence of the solid *FeOOH*(s). The dissolution of *FeOOH*(s) is described by:

$$FeOOH(s) = Fe^{3+} - 3H^+ + 2H_2O(l),\ K_{sp} = 3.428 \quad (3\text{-}4)$$

The formation of complex $Fe(OH)_3$(aq) is described by:

$$Fe^{3+} - 3H^+ + 3H_2O(l) = Fe(OH)_3(aq),\ K_f = 6.707 \cdot 10^{-13} \quad (3\text{-}5)$$

These expressions can be combined to produce:

$$FeOOH(s) + H_2O(l) = Fe(OH)_3(aq),\ K_{sp}' = [Fe(OH)_3(aq)] = 2.299 \cdot 10^{-12} \quad (3\text{-}6)$$

Thus, in the presence of *FeOOH*(s), the concentration of $Fe(OH)_3$(aq) (equal to stet activity because of zero charge) must remain constant at the value $2.299 \cdot 10^{-12}$ M regardless of conditions of either *pH* or *Eh*. This can be seen in the results shown in Fig. 3.8; because both inflowing and domain solutions were required to be at equilibrium with *FeOOH*(s), the concentration of $Fe(OH)_3$(aq) throughout the domain never varies from the value given by Eq.(3-6).

3.2 Comparison of different model applications to the uranium-iron redox system

The numerical simulations of the dynamical system were done by the directly coupled code THCC and the sequentially coupled code MCOTAC[4]. The transport parameters are listed in

---

[4] For a detailed description of the codes and the used numerical algorithms the reader is referred to [Carnahan, 1986] and [Pfingsten, 1994].

Tab. 3.4. For THCC calculations a spatial grid size of 0.2 m was chosen and the time step size was variable, depending on the convergence behaviour during calculation. MCOTAC calculations were done with the same transport parameters, a maximum particle number of 50000 and a maximum time step size of 210 s (defined by the chosen spatial grid size (0.2 m) and the transport parameter (MCOTAC, [Pfingsten, 1994]). The total migration time for the simulation was limited to 8000 s, so that an inert tracer did not migrate through the whole model domain during that time, and boundary effects were negligible.

Table 3.4: Transport parameters used in the uranium-iron simulations

flow velocity	0.001 m/s
dispersivity	0.05 m
diffusion coefficient	$1 \cdot 10^{-9}$ m²/s
domain length	10 m

The numerical problem which occurred in the dynamic modelling is the sharp redox front which migrates through the spatial domain, accompanied by steep gradients of species concentrations. In figures 3.1 to 3.8 the concentration profiles of the basis species, complexes and solids calculated by THCC and MCOTAC are compared at different migration times. Generally the profiles are in good agreement. But these profiles can be divided into three groups, two for the solute concentrations and one for the solid concentration. For the basis species UO_2^{2+}, Fe^{3+} and H^+, THCC produces oscillations within the profiles (most noticeable on a linear concentration scale in Fig. 3.1). The concentration profiles of the complex $UO_2(CO_3)_2^{2-}$ (Fig. 3.5) show the same behaviour as the related profiles of the basis species UO_2^{2+} (Fig. 3.1). The location of these oscillations coincides with the UO_2(s) precipitation front (Figures 3.4 and 3.8) where a chemical system change takes place. This difficulty could arise within any directly coupled code using a finite difference formulation. (For finite difference formulations such overshooting or oscillations indicate an incorrectly adjusted system [Gresho & Lee, 1981], which is a difficulty in a non-linear coupled formulation with highly varying source terms). These oscillations did not occur for the basis species Fe^{2+}, CO_3^{2-} and Na^+ (Figures 3.2, 3.3 and 3.4) although Fe^{2+} takes part in redox reactions with the basis species which show the oscillating behaviour.

The second group of profiles shows very few discrepancies between the codes. The fronts are at the same positions, and the profile shapes are identical if the fluctuations in the 'zigzag' formed curves produced by the multiple particle random walk description (MCOTAC) are neglected (Figures 3.2, 3.3 and 3.4). The reason for these 'zigzag' curves is the varying number of particles present in neighbouring grid cells in subsequent time steps,

and related to this a varying species concentration within the grid cell[5]. The profiles calculated by MCOTAC show a slightly more dispersive form. This is the consequence of sequential coupling of transport and chemical equilibrium calculations, where after each transport step the species masses transported by particles are smeared out over the grid cell for chemical equilibrium calculation. In addition, a variation of the fronts with respect to their location is caused by the low amount of the solid UO_2(s) precipitated. This amount and the varying number of particles can dissolve (or precipitate) the whole UO_2(s) amount in a grid cell from one time step to another. These variations can lead to a forward or backward movement of the redox front with respect to individual grid cells. This is another source for differences in the calculated profiles for the basis species UO_2^{2+} (Fig. 3.1), Fe^{3+} (Fig. 3.2), and H^+ (Fig. 3.3). The fact that the Fe^{2+}, $CO_3^{2-}$and Na^+ profiles are in good agreement underlines that the differences near the redox front are mostly due to the overshooting of THCC calculations.

Minor differences between the calculated profiles become obvious only in Figures 3.1 and 3.8 on a logarithmic scale. The concentration profiles of the basis species UO_2^{2+} (and related complexes) calculated by THCC are located further into the domain than those calculated by MCOTAC. This difference occurs only for UO_2^{2+}[6] (and related complexes) where the initial concentrations were set to zero within the domain. This spreading of the two profiles with increasing distance is due to a higher numerical dispersion for the finite difference formulation within THCC than for a sequential coupled formulation using a random-walk description for transport (MCOTAC), and should be kept in mind if comparable initial or boundary conditions must be defined.

---

[5] This is a general phenomenon within a random walk transport description which can be reduced by increasing the number of particles in the domain [Prickett, Naymik & Lonnquist, 1982; Kinzelbach, 1987] . Here, the limit is 50000 particles due to computer resources, and variations between 10000 particles (minimum number required) and 50000 particles showed no significant changes in the fluctuations of the 'zigzag' profiles calculated by MCOTAC.

[6]Although this operational concentration of the basis species UO_2^{2+} is at chemically meaningless levels, the comparison of the numerical behaviour of both codes is of importance for comparable coupled systems with similar boundary and initial conditions.

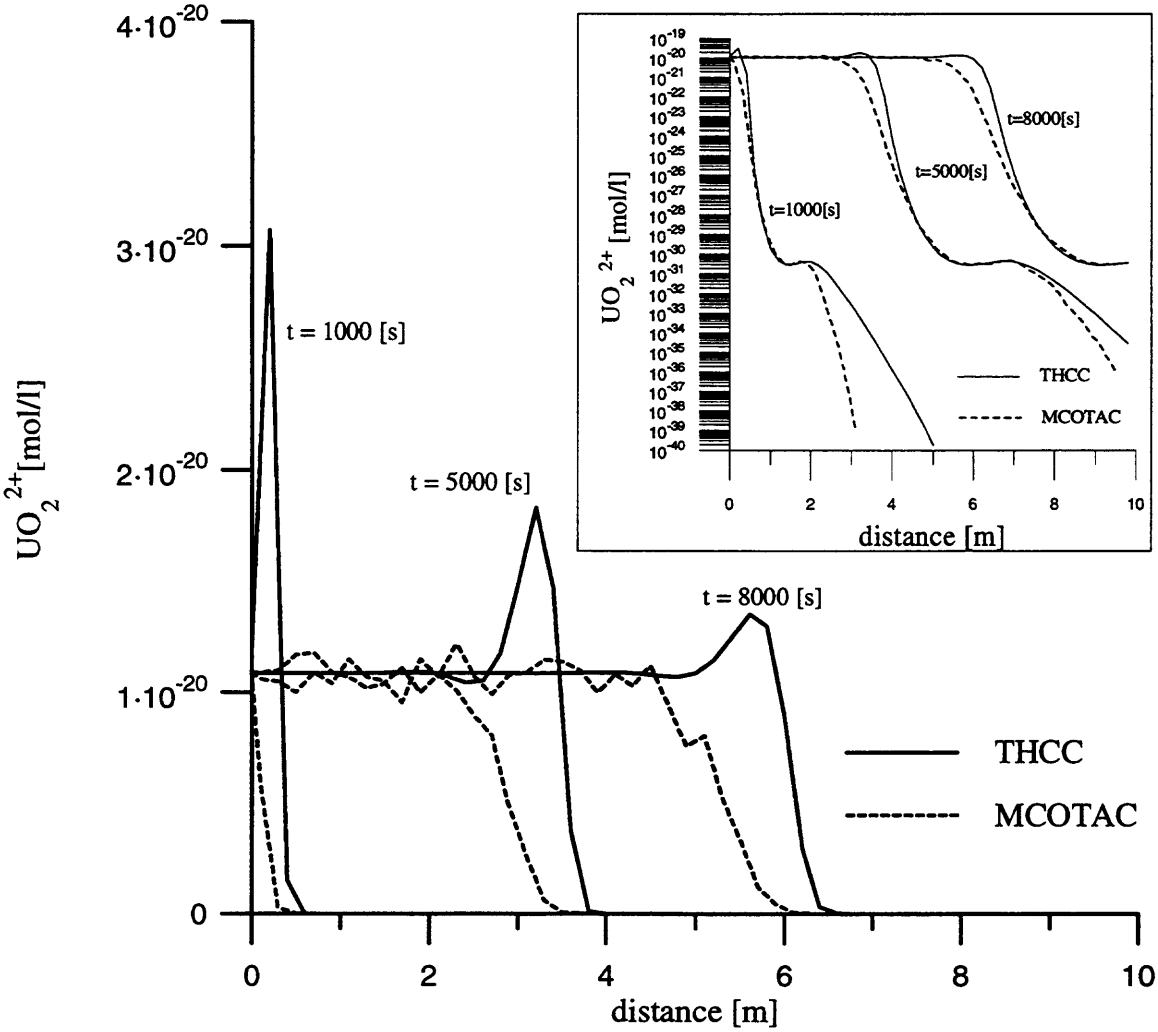

Figure 3.1: Comparison of the operational[7] UO_2^{2+} concentration profiles at 1000 s, 5000 s and 8000 s of migration calculated by THCC and MCOTAC on a linear and logarithmic scale.

[7]The chemical unreasonable (operational) concentrations for some basis species are a consequence of the chosen set of basis species used to formulate the redox system. Such species do not transport any chemical mass but their formal concentrations are relevant within the numerical scheme. The sensitivity of the numbers is used to demonstrate differing features of the two codes.

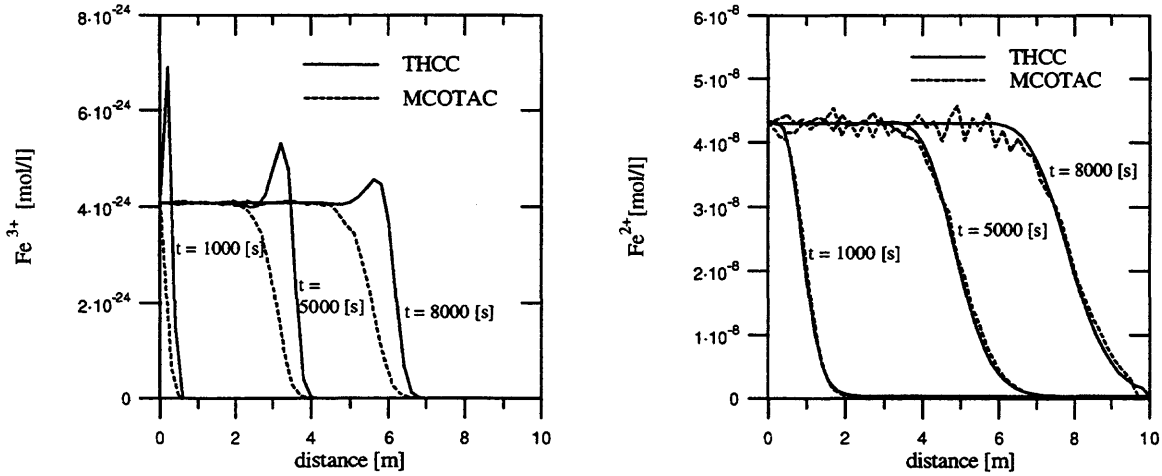

Figure 3.2: Comparison of the concentration profiles of the basis species Fe^{3+}[8] and Fe^{2+} calculated by THCC and MCOTAC for different migration times.

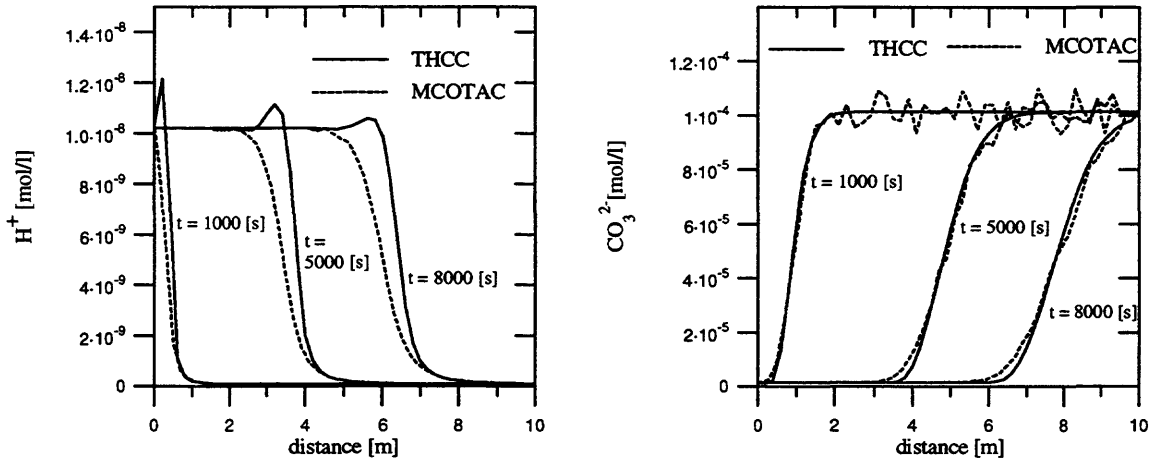

Figure 3.3: Comparison of the concentration profiles of the basis species H^+ and CO_3^{2-} calculated by THCC and MCOTAC for different migration times.

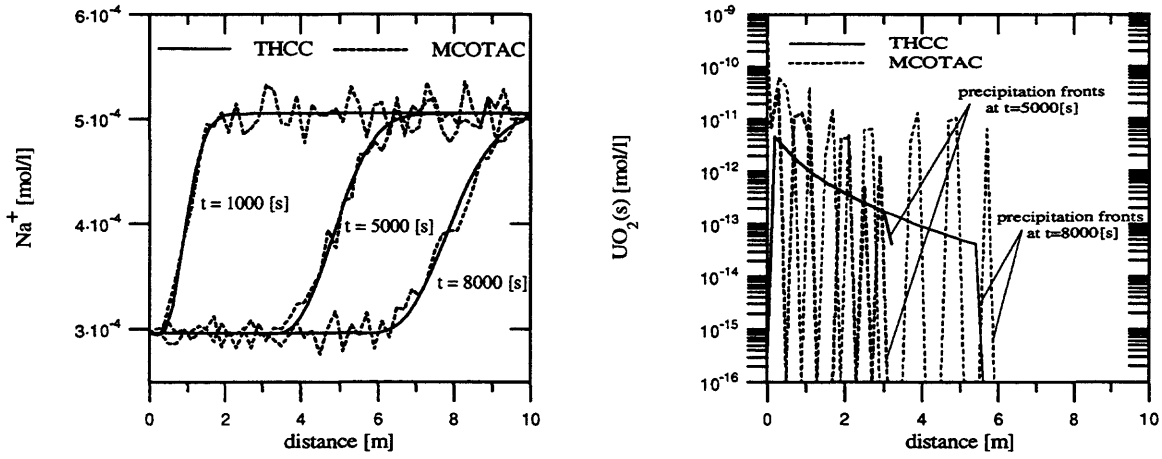

Figure 3.4: Comparison of the concentration profiles of the basis species Na^+ and the solid $UO_2(s)$ calculated by THCC and MCOTAC.

---

[8]Operational concentration, see footnote 6

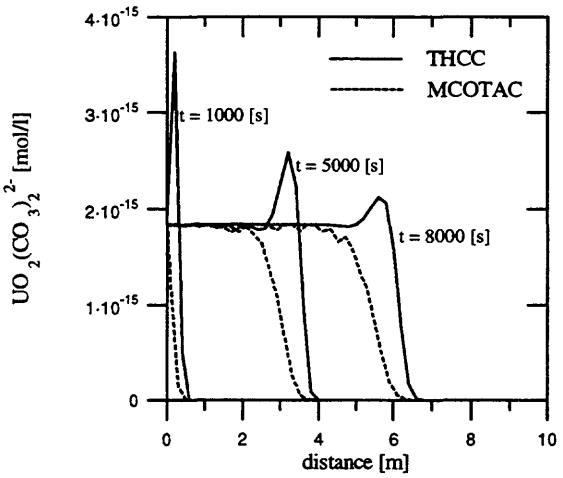

Figure 3.5: Comparison of the concentration profiles of the complex $UO_2(CO_3)_2^{2-}$ [9] calculated by THCC and MCOTAC. THCC calculations show the same oscillation behaviour as calculated for the basis species UO_2^{2+} (Fig. 3.1).

Investigation of the oscillating behaviour of THCC calculations shows that the oscillation decreases if the dispersivity is increased from 0.05 m (original value) to 0.08 m. The physical system changes with higher dispersivity because of a changing transport parameter. The result is a more dispersive concentration profile if pure tracer transport is concerned. Trying to model the same physical system with a finer grid (0.1 m compared to 0.2 m before) caused convergence problems within THCC calculations in form of a decreasing time step size during the dynamic calculation. So, the CPU time increased to unacceptable values. For 5000 s of migration, which takes about three days of CPU time, and after which the calculation was aborted, the UO_2^{2+} concentration profile is calculated for a 100 node grid (Fig. 3.6). This profile does not show the oscillating behaviour but is closer to the MCOTAC calculated profile (dispersivity = 0.05 m) and the THCC calculated profiles at higher dispersivities (0.06 m, 0.07 m and 0.08 m)[10]. But for the THCC calculation with the fine grid, the $UO_2(s)$ precipitation occurs only at the first two nodes up to x = 0.1 m. For the coarse grid this precipitation reached nodes 10 to 16 (x = 2.0 m to 3.2 m) that means an increasing redox front movement for smaller dispersivities. This mismatch of the front position reflects convergence problems within THCC calculations for the fine grid.

The decreasing oscillations for higher dispersivities may be explained by a smoother redox front (smearing out at higher dispersivities). This argument is underlined by the fact that the oscillations decreased also with migration time, which includes a smearing out of the redox front with time as seen for the three concentration profiles at 1000 s, 5000 s and 8000 s in Figures 3.1 to 3.3 and 3.5. A full understanding of this effect requires further investigations (see Chapter 4.2.4). As seen in Fig. 3.6 the concentration profiles of UO_2^{2+} are calculated correctly for higher dispersivities, which produce more dispersive profiles. This results in

---

[9]Operational concentration, see footnote 6

[10]The increasing dispersivity is accompanied by a smaller Peclet number *Pe* (see Chapter 4.2.5) defined within advective-dispersive transport (Kinzelbach, 1987). In this case *Pe* decreases from 4 to 2.5 as the dispersivity increases from 0.05 m to 0.08 m. (see Eq. 4-10 and related discussion)

slightly lower concentrations to the left of the redox front and higher concentrations to the right. In Fig. 3.6 only the upper part of the concentration profile is shown on a linear scale, therefore, only the lower concentrations to the left of the front are obvious, whereas the higher concentrations to the right are not visible on this scale (see Fig. 3.1).

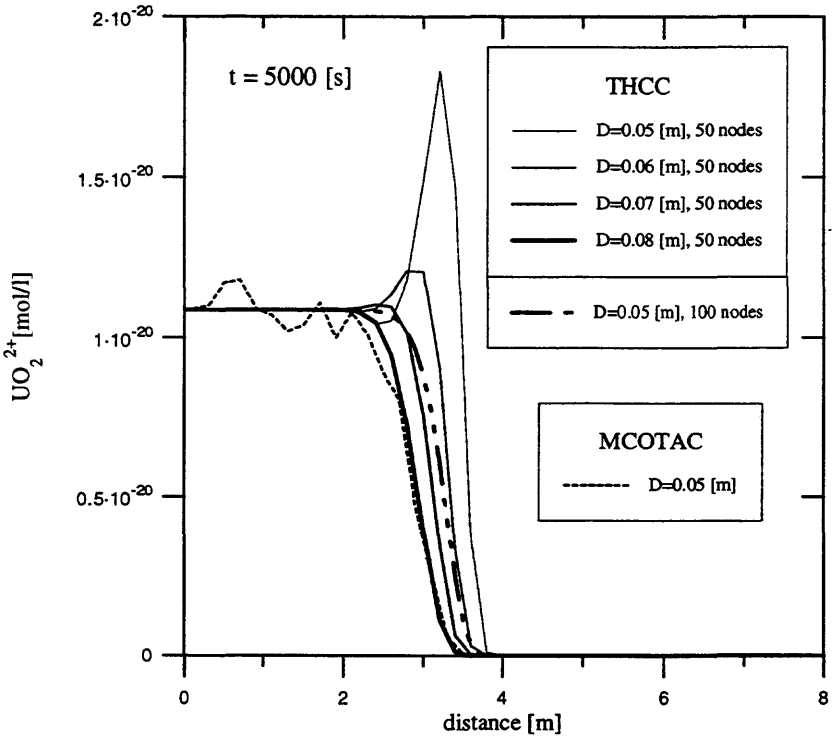

Figure 3.6: Influence of the dispersivity on the UO_2^{2+}[11] concentration profiles calculated by THCC. The grid size was 0.2 m (50 nodes) and 0.1 m (100 nodes).

Major differences between the two calculations occurred for the UO_2(s) solid concentration profiles (Figures 3.4 and 3.7). UO_2(s) precipitation is coupled to $U(OH)_4$(aq) concentration which must remain constant at the value $4.079 \cdot 10^{-10}$ mol/l when UO_2(s) is present (see Eq. 3-3). Here, the random walk transport description (MCOTAC) is accompanied by fluctuations in the $U(OH)_4$(aq) concentration profile. This causes the UO_2(s) concentration (only present at a low concentration level comparable to other uranium complex concentrations in solution) to vary over several orders, including zero solid concentration within a region of UO_2(s) precipitation, where this solid is present at neighbouring cells. At solid concentration levels of $10^{-10} - 10^{-11}$ mol/l for UO_2(s) and concentrations of uranium bearing ions, especially $U(OH)_4$(aq) in the range of $4.079 \cdot 10^{-10}$ mol/l, the solid UO_2(s) did not serve as a buffer for the solute $U(OH)_4$(aq) or other uranium bearing complexes within a

[11]Operational, see footnote 6

random-walk description[12]. In the case of THCC calculations, the iteration between transport and chemical equilibrium calculations prevent such oscillations in the solid concentration, and the UO_2(s) profile results in a smooth curve. If only the region of UO_2(s) precipitation is compared for different migration times, then the precipitation fronts coincide (Fig. 3.7).

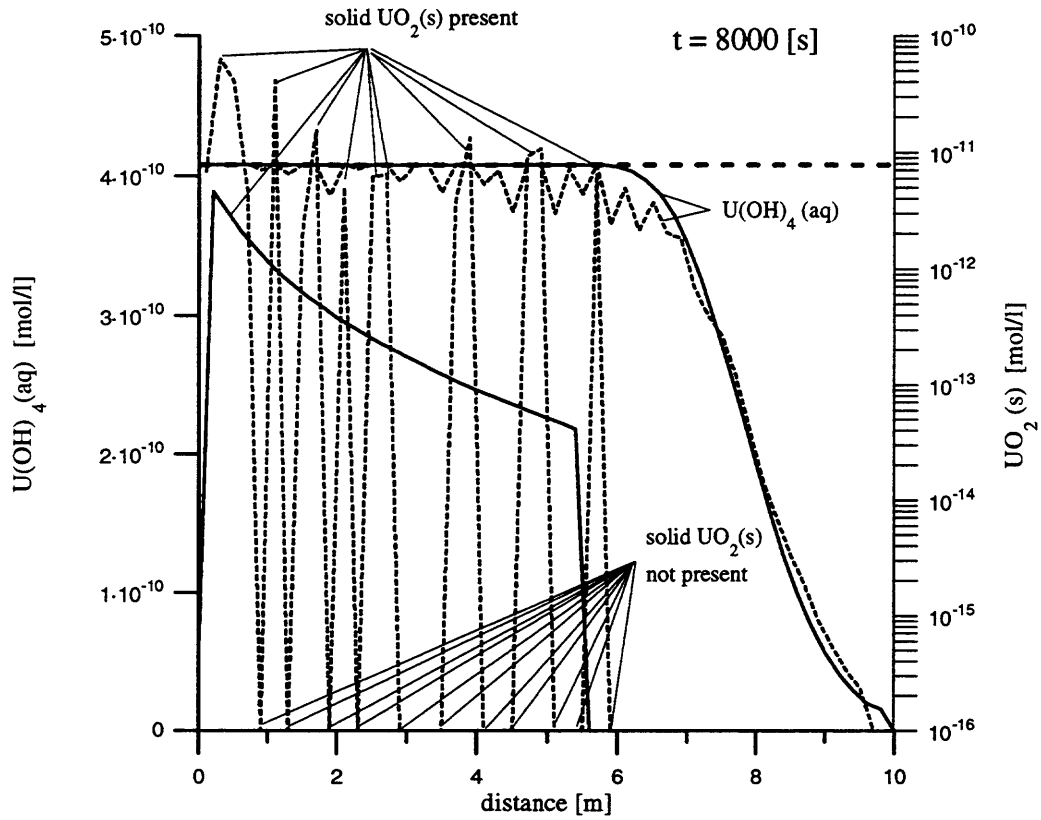

Figure 3.7: Relation between the varying $UO_2(s)$ solid concentration and the $U(OH)_4(aq)$ concentration within the MCOTAC calculations (dashed lines). Below a $U(OH)_4(aq)$ concentration limit of $4.079 \cdot 10^{-10}$ mol/l (dashed horizontal line), no $UO_2(s)$ solid was present (see text).

As a summary comparison, all species concentration profiles at a migration time of 5000 s were plotted on a logarithmic scale (Fig. 3.8). This again shows a good agreement of the

---

[12]If the solid UO_2(s) is present at a much higher level than the uranium bearing ions in solution, the total mass of uranium is defined predominantly by the amount of UO_2(s) in each grid cell. Then the uranium transported in between the cells within the solute is negligible compared to the total amount of uranium in the cells. This means a constant $U(OH)_4$(aq) concentration at $4.079 \cdot 10^{-10}$ mol/l for the system defined above buffered by a high amount of UO_2(s). In the case modelled here, the uranium is predominantly defined by the concentration of the uranium bearing ions in solution, especially $U(OH)_4$(aq), which is varying for the random walk description. If the fluctuations cause a $U(OH)_4$(aq) concentration below $4.079 \cdot 10^{-10}$ mol/l, complete dissolution of the solid UO_2(s) in one grid cell, and a precipitation in the neighbouring cell can be observed for MCOTAC calculations.

two different coupled code calculations with small differences near the redox front and for uranium bearing species near the right boundary (as discussed before).

Finally the used CPU times for the calculation of the uranium-iron redox system are compared in Tab. 3.5 for a migration time of 8000 s on two available hardware platforms. It can be seen that there are no large differences in CPU time, which is influenced by parameter definitions for each calculation (grid size, time stepping, output control etc.). For this tricky system the time used for calculation is only 30 to 270 times faster than the simulated "experimental migration time" of 8000 s. In order to have the chosen time and space resolution for the calculated concentration profiles this CPU time must be accepted up to now. MCOTAC calculation reached times down to 30 s which is promising for further development.

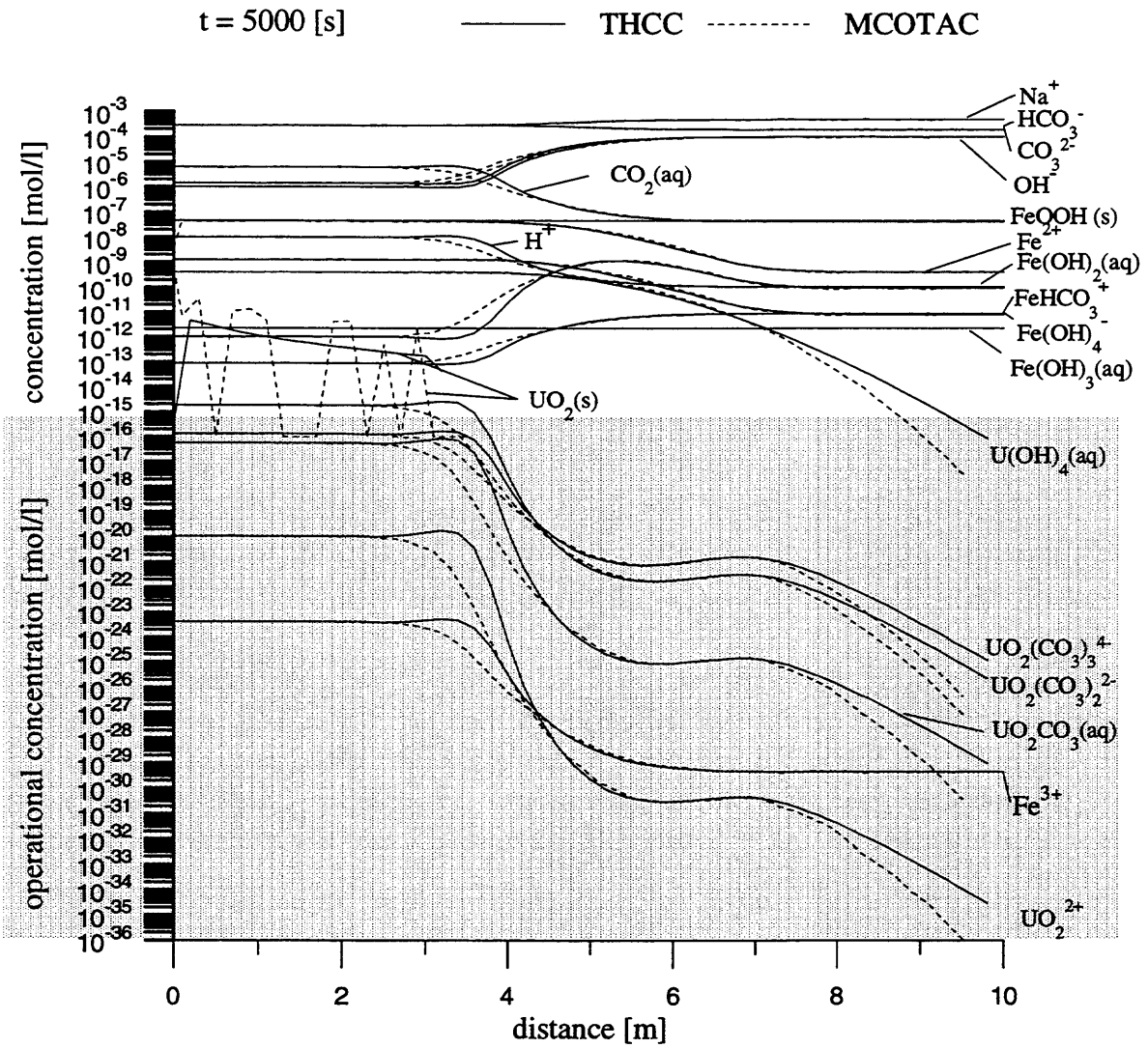

Figure 3.8: Concentration profiles calculated by THCC and MCOTAC for all species (solutes and solids) included in the system (species concentration in the shadowed area are without a chemical meaning but are used in the mathematical scheme and are given for completeness).

Table 3.5: CPU time used for different coupled code calculations on two different computer systems for a migration time of 8000 s. The listed times depend on several code options such as amount of output data, convergence criteria, number of particles, etc. and give a rough comparison.[13]

Computer	THCC [s]	MCOTAC [s]
Titan Kubota 3020	120 - 195	~ 30 - 200
Intel i860 inboard in '486 PC	~ 280	~ 60 - 310

4. Simulation of uranium-hydrogen redox systems

4.1 Definition of the system

In the uranium-hydrogen system, a solution containing uranium at $Eh = 0.1$ V and $pH = 8$ flows into a spatial domain occupied by a solution devoid of uranium and initially at $Eh = -0.45$ V and $pH = 10$. Both inlet and domain solutions contain carbonate, as CO_2(aq), HCO_3^-, and CO_3^{2-}, at a total aqueous concentration of $3 \cdot 10^{-4}$ M. The inflowing solution is at equilibrium with the solid $UO_2(OH)_2 \cdot H_2O(s)$ (schoepite). In all simulations the master reductant is H_2(aq). All simulations allow precipitation of solids $UO_2(OH)_2 \cdot H_2O(s)$ and UO_2(s) (uraninite), and include the formation of aqueous phase complexes $CO_2(aq)$, CO_3^{2-}, UO_2OH^+, $UO_2CO_3(aq)$, $UO_2(CO_3)_3^{4-}$, $U(OH)_4$(aq). Water dissociation is also included.

The precipitation of solids and the formation of complexes are written in terms of a set of the basis species $UO_2(CO_3)_2^{2-}$, HCO_3^-, H_2(aq), OH^-, Na^+ (see Tab. 4.1) that is the minimum number of independent variables to describe the system at chemical equilibrium. Here, major ions are used as basis species to describe the system.

In this system, the master redox couple is H_2O(aq)-H_2(aq). The half-cell reaction for the reduction of H_2O(l) to H_2(aq) is:

$$2H_2O(l) + 2e^- = H_2(aq) + 2OH^-,\ E° = -0.9198 \text{ V} \qquad (4\text{-}1)$$

Then the Eh is given by:

$$Eh = -0.9198 - 0.02958 \log([H_2(aq)][OH^-]^2) \qquad (4\text{-}2a)$$

---

[13] In the case of THCC calculation for a grid size of 0.1 m (100 nodes) the CPU time increased to some days to calculate up to a migration time of 5000 s. Convergence problems, and the related internal decreasing of the time step in the dynamic calculation caused a break before reaching the migration time of 8000 s.

$$Eh = -0.9198 - 0.05916\log[OH^-] - 0.02958\log[H_2(aq)] \quad (4\text{-}2b)$$

$$Eh = -0.9198 - 0.05916(-13.9954 - \log[H^+]) - 0.02958\log[H_2(aq)] \quad (4\text{-}2c)$$

$$Eh = -0.0918 - 0.05916pH - 0.02958\log[H_2(aq)] \quad (4\text{-}2d)$$

Eq.(4-2d) is identical to Eq.(2-9). If H^+-H_2(aq) is chosen to be the master redox couple, then the *Eh* in these systems is given by Eqs. (2-9) and (4-2d).

Table 4.1: Chemical reactions and equilibrium constants (at 25° C) described by the set of basis species (see footnote 1).

reaction	logK
$H_2O(l)$ - OH^- = H^+	–13.9954
HCO_3^- - OH^- = CO_2(aq)	–7.65055
$HCO_3^- + OH^- - H_2O(l) = CO_3^{2-}$	3.66658
$UO_2(CO_3)_2^{2-} - 2HCO_3^- - OH^- + 2H_2O(l) = UO_2OH^+$	–15.5158
$UO_2(CO_3)_2^{2-} - HCO_3^- - OH^- + H_2O(l) = UO_2CO_3\ (aq)$	–11.0217
$UO_2(CO_3)_2^{2-} + HCO_3^- + OH^- - H_2O(l) = UO_2(CO_3)_3^{4-}$	8.28131
$UO_2(CO_3)_2^{2-} - 2HCO_3^- + H_2\ (aq) + 2H_2O(l) = U(OH)_4\ (aq)$	11.2913
$UO_2(OH)_2 \cdot H_2O\ (s) = UO_2(CO_3)_2^{2-} - 2HCO_3^- + 3H_2O(l)$	1.14556
$UO_2\ (s) = UO_2(CO_3)_2^{2-} - 2HCO_3^- + H_2(aq)$	–20.6807

The chemical system was set up so that near the influx boundary a reduction of *U*(VI) species causes concentrations of the *U*(IV) complex, $U(OH)_4$(aq), to rise to the value $4.08 \cdot 10^{-10}$ M, after which the *U*(IV) solid, UO_2(s), precipitates (see Eq. (3-3) and accompanying discussion). Concurrently, the concentration of H_2(aq) near this boundary decreases until it reaches $1.492 \cdot 10^{-22}$ M, and the *U*(VI) solid $UO_2(OH)_2 \cdot H_2O(s)$, starts to precipitate (see Fig. 4.1). This can be understood by considering the reactions for dissolution of $UO_2(OH)_2 \cdot H_2O(s)$ and UO_2(s).

$$UO_2(OH)_2 \cdot H_2O(s) = UO_2(CO_3)_2^{2-} - 2HCO_3^- + 3H_2O(l),\ \log K_{sp} = 1.14556 \quad (4\text{-}3)$$

$$UO_2(s) = UO_2(CO_3)_2^{2-} - 2HCO_3^- + H_2(aq),\ \log K_{sp} = -20.6807 \quad (4\text{-}4)$$

Combining reaction (4-3) with (4-4) produces:

$$UO_2(OH)_2 \cdot H_2O(s) + H_2(aq) = UO_2(s) + 3H_2O(l),\quad \log K_{sp} = -\log[H_2(aq)] = 21.82626 \quad (4\text{-}5)$$

Then the two solids coexist when $[H_2(aq)] = 1.492 \cdot 10^{-22}$ M and the solubility products are satisfied simultaneously. $[H_2(aq)]$ maintains this value along a straight line in *Eh-pH* space (Fig. 4.1). The equation of the line is given directly by substituting $[H_2(aq)] = 1.492 \cdot 10^{-22}$ M into Eq. (4-2d). Alternatively, the equation can be derived by writing the reduction of $UO_2(OH)_2 \cdot H_2O(s)$ to UO_2(s), using H^+ as a basis species:

$$UO_2(OH)_2 \cdot H_2O(s) + 2e^- + 2H^+ = UO_2(s),\ E° = 0.5538\ [\text{v}] \qquad (4\text{-}6)$$

Then, when $[H_2(aq)] = 1.492 \cdot 10^{-22}$ M, *Eh* and *pH* are related by:

$$Eh = 0.5538 - 0.05916\,pH \qquad (4\text{-}7)$$

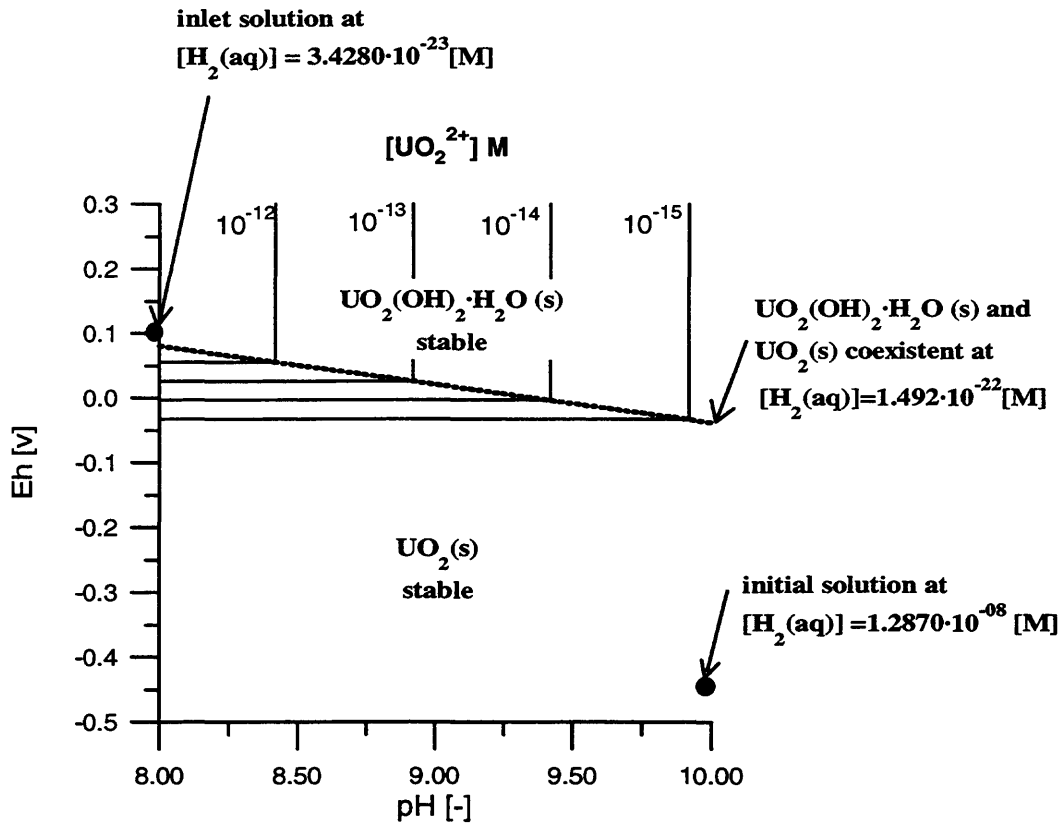

Figure 4.1: *Eh-pH diagram for schoepite and uraninite in equilibrium with the solute UO_2^{2+} (contour lines of constant activities) in U-H-O system used in Chapt. 4.2; only oxidation states IV and VI are included. Other solids are omitted from the diagram, such as $U_2O_3(s), UO_2CO_3(s)$, etc. Uranium concentrations are defined for inlet (upper left dot) and initial solution (lower right dot) so that the inlet solution is saturated with respect to $UO_2(OH)_2 \cdot H_2O(s)$, where for the initial solution no solid is present. In the dynamic system, first the solid $UO_2(s)$ precipitates in the domain due to reduction of U(VI) near the inlet boundary ($U(OH)_4(aq)$ rises to a value of $4.08 \cdot 10^{-10}$ M). Then the $H_2(aq)$ concentration decreases, and both solids coexist at $[H_2(aq)] = 1.492 \cdot 10^{-22} M$.*

Transport parameters are given in Tab. 4.2. The number of spatial nodes (51) is the same in all cases. The grid length was 10 m for a spacing of 0.2 m; and respectively, 20 m for a spacing of 0.4 m. Within MCOTAC calculations 30000 particles are used for the random walk transport description.

Table 4.2: Transport parameters used in all uranium-hydrogen simulations

flow velocity	0.0005 m/s
dispersivity	0.05 m
diffusion coefficient	$1 \cdot 10^{-9}$ m²/s

In addition to the general comparison of the results of both codes, the comparison of the two codes includes a sensitivity analysis on individual code calculations depending on the following parameter changes:

- influence of set of basis species
- influence of boundary conditions
- influence of spatial grid spacing

4.2 Comparison of different model applications to uranium-hydrogen redox systems

In the following sections different uranium-hydrogen redox systems are modelled by THCC and MCOTAC and the results are compared. The objective was, besides a general comparison of the results of the two calculations methods, an investigation of the influence of parameter changes on the produced results by both codes.

4.2.1 Simulation of the uranium-hydrogen system

For the uranium-hydrogen system described in Chapt. 4.1 the simulated migration time is 10000 s. The concentrations of the basis species for the inlet solution and the initial domain solution are given in the following tables:

Table 4.3: Inlet concentration of basis species in solution and amount of solid used to specify the inlet solution (see footnote 1)[14]*. (The solid concentration is given for completeness to allow comparison to codes using total basis species concentration.)*

Basis species and solids	total aqueous concentration [mol/l]	species concentration [mol/l]
$UO_2(CO_3)_2^{2-}$	$1.3701 \cdot 10^{-6}$	$1.2412 \cdot 10^{-6}$
HCO_3^-	$3.0000 \cdot 10^{-4}$	$2.9217 \cdot 10^{-4}$
H_2(aq)	$8.9647 \cdot 10^{-11}$	$3.2800 \cdot 10^{-23}$
OH^-	$-3.8168 \cdot 10^{-6}$	$1.0310 \cdot 10^{-6}$
Na^+	$2.9892 \cdot 10^{-4}$	$2.9892 \cdot 10^{-4}$
$UO_2(OH)_2 \cdot H_2O(s)$	present at $2.9869 \cdot 10^{-8}$	-
UO_2(s)	-	-

Table 4.4: Initial concentrations of basis species in solution and amount of solid in the spatial domain (see footnote 1).

Basis species and solids	total aqueous concentration [mol/l]	species concentration [mol/l]
$UO_2(CO_3)_2^{2-}$	0	0
HCO_3^-	$3.0000 \cdot 10^{-4}$	$1.9866 \cdot 10^{-4}$
H_2(aq)	$1.2870 \cdot 10^{-8}$	$1.2870 \cdot 10^{-8}$
OH^-	$2.0525 \cdot 10^{-4}$	$1.0400 \cdot 10^{-4}$
Na^+	$5.0525 \cdot 10^{-4}$	$5.0525 \cdot 10^{-4}$
$UO_2(OH)_2 \cdot H_2O(s)$	-	-
UO_2(s)	-	-

A general comparison of the calculated profiles calculated by THCC and MCOTAC is presented in Figures 4.2 to 4.6. The concentration profiles of the basis species $UO_2(CO_3)_2^{2-}$, HCO_3^-, H_2(aq) and OH^- are in good agreement (Figures 4.2 and 4.3). The sharp fronts produced by the redox front were reproduced by both codes. The

[14]Negative total concentration of a basis species is possible depending on the chosen set of basis species. It has no direct chemical meaning but it is a result of the numerical scheme.

concentration profiles showed only some discrepancies due to fluctuations coming with the random walk transport description within MCOTAC. These random fluctuations can be decreased by increasing the number of particles within the MCOTAC calculation but this will increase the computing time and the computer memory. The non-random oscillating behaviour of the THCC calculated profiles did not appear for the basis species as intensive as in the uranium-iron redox system (Chapt. 3.2). Only small oscillations appeared within the HCO_3^- profile at the left (high concentration level) side of the front(Fig. 4.2).

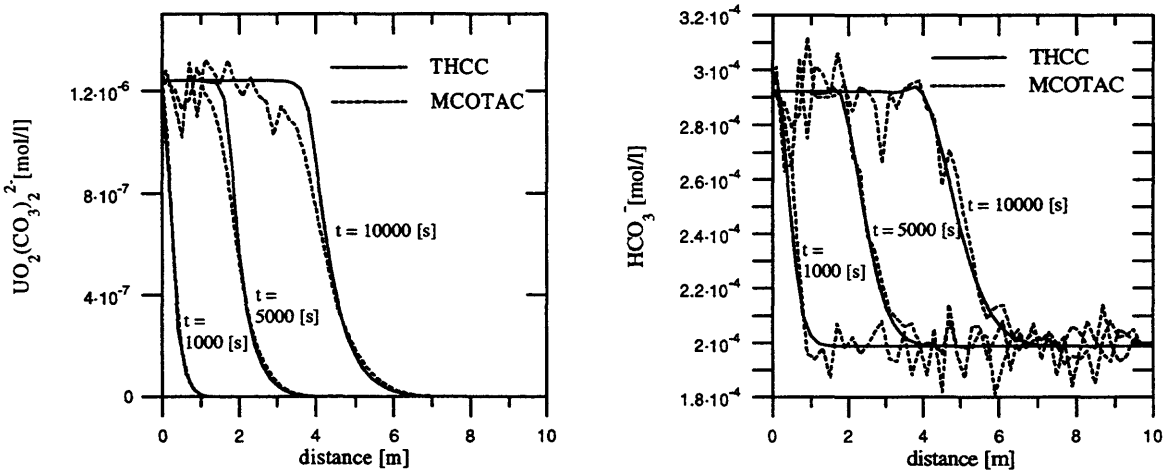

Figure 4.2: Comparison of concentration profiles for basis species $UO_2(CO_3)_2^{2-}$ and HCO_3^- calculated by THCC and MCOTAC.

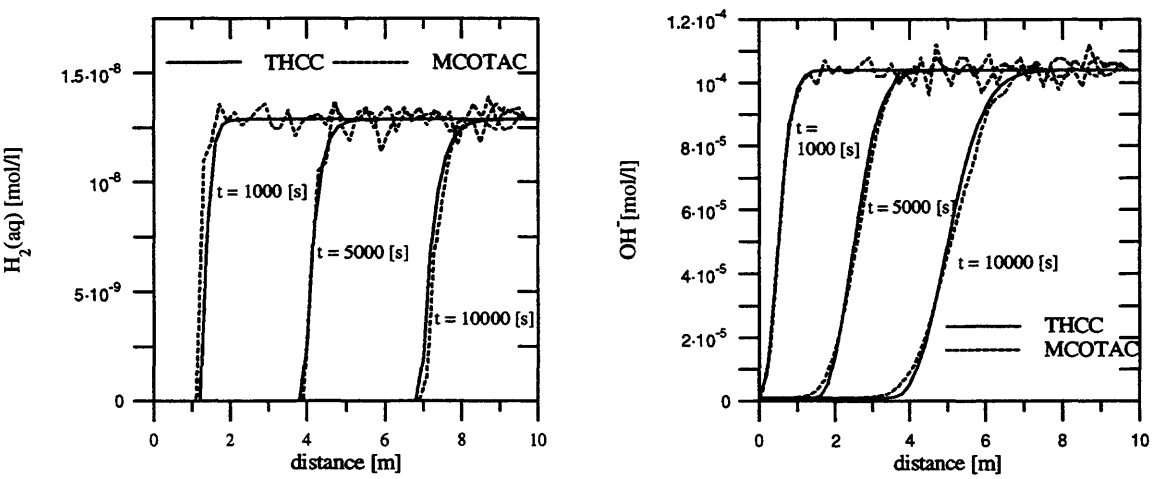

Figure 4.3: Concentration profiles for basis species $H_2(aq)$ and OH^- calculated by THCC and MCOTAC.

Oscillating profiles for this simulation are more noticeable within the concentration profiles of the complexes H^+ and $UO_2CO_3(aq)$ (Fig. 4.4) and exceed the random fluctuations within the MCOTAC calculated profiles. The apparent steeper fronts of the THCC profiles are due to the numerical artifact of these oscillations. The profiles would be closer together

without these oscillations. It is also noticed that the oscillations coincide here with the precipitation front of the solid $UO_2(OH)_2 \cdot H_2O(s)$, and not with the redox front and related precipitation of $UO_2(s)$, as it was observed in Chapt. 3.2.

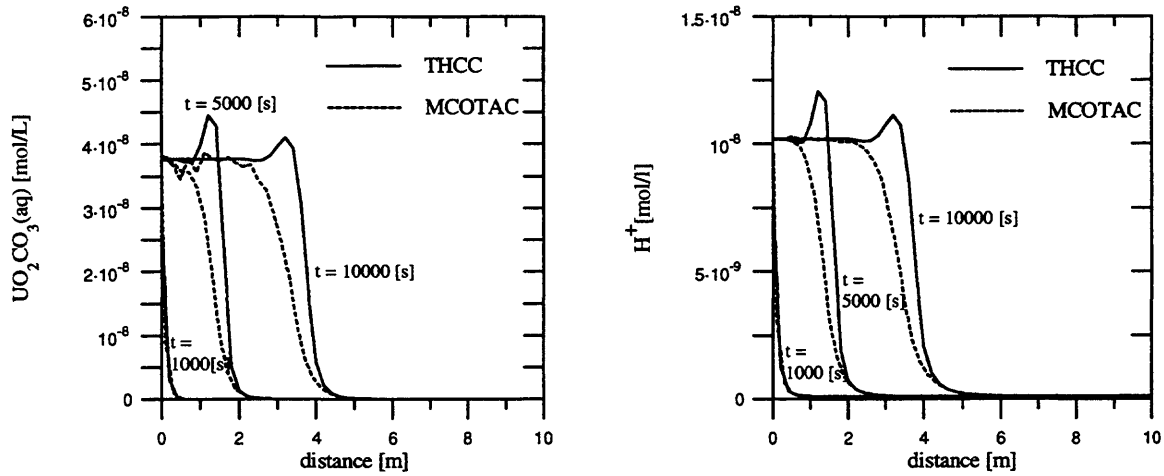

Figure 4.4: Comparison of the concentration profiles of complex species $UO_2CO_3(aq)$ and H^+ calculated by THCC and MCOTAC.

The $UO_2(CO_3)_3^{4-}$-profiles showed oscillations at a lower level near the left side of the pulse shaped front. In between the UO_2(s) and the $UO_2(OH)_2 \cdot H_2O(s)$ precipitation front the concentration of the U(VI) complex $UO_2(CO_3)_3^{4-}$ rises up to a maximum level (Fig. 4.6) up to the region where H_2(aq) reaches $1.492 \cdot 10^{-22}$ M. Then the $UO_2(CO_3)_3^{4-}$ concentration decreases simultaneously with precipitation of the U(VI) solid, $UO_2(OH)_2 \cdot H_2O(s)$ and becomes constant at the inlet concentration of $UO_2(CO_3)_3^{4-}$. These pulse-shaped profiles were calculated equally by both codes. They agree in form and height. Small differences occurring at the left sides of the pulse maxima are directly correlated to the calculated oscillating profiles by THCC and with the $UO_2(OH)_2 \cdot H_2O(s)$ precipitation front. The leading part of the pulse coincides with the precipitation of the solid $UO_2(s)$, and the related redox front. The left side of the pulse-shaped profile coincides with precipitation of the solid $UO_2(OH)_2 \cdot H_2O(s)$.

No oscillations appeared for the complex $U(OH)_4(aq)$ (Figure 4.5) whose aqueous concentration is defined by the solid $UO_2(s)$ (Eq. 3-3). In contrast to Chapt. 3.2, here the $U(OH)_4(aq)$ profile does not show fluctuations, and the MCOTAC profiles coincide with the THCC profiles, constant on a plateau (defined by the solid $UO_2(s)$) up to the redox front. Therefore, it becomes obvious that the $UO_2(s)$ profile calculated by MCOTAC does not show high fluctuations between solid present and solid not present as for the uranium-iron system (Fig. 3.7). Here, the fluctuations are much smaller and the $UO_2(s)$ profile calculated by MCOTAC fluctuates around the THCC calculated profile but the solid is always present. The oscillations in the concentration profiles calculated by THCC coincide in each case with the precipitation front of a solid; here, it is the precipitation of the U(VI)

solid, $UO_2(OH)_2 \cdot H_2O(s)$ (Figure 4.6). They do not coincide necessarily with the redox front which is underlined by the last example. The precipitation of the U(IV) solid, UO_2(s), causes no oscillations as in Chapt. 3.2 for the uranium-iron redox system, although this precipitation front is related to the redox front in the uranium-hydrogen system too. In the uranium-iron system only one front system (solid and redox) was present, while in this uranium-hydrogen system two moving fronts (Fig. 4.6) can be observed where only one of them is related to the redox front.

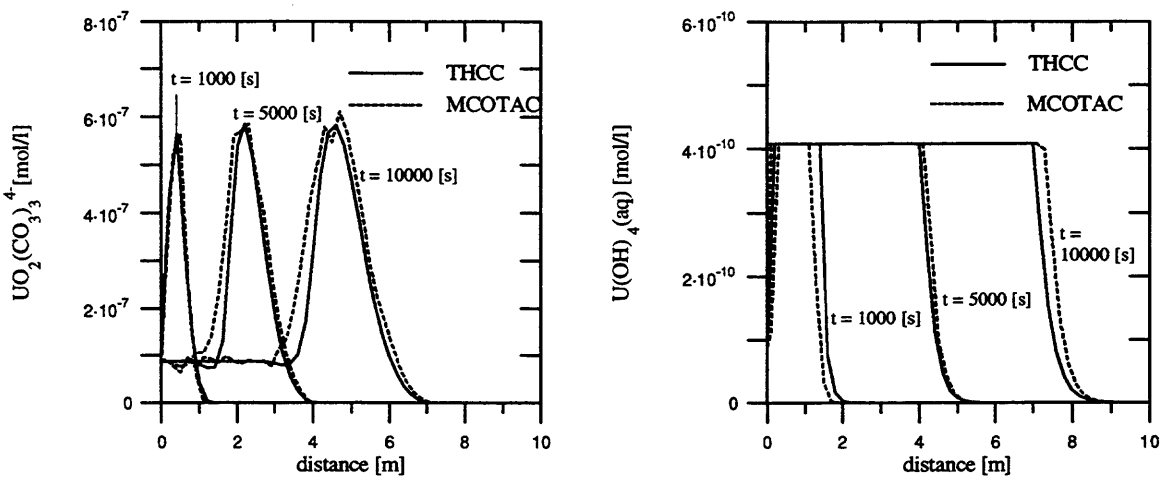

Figure 4.5: Comparison of the concentration profiles of complex species $UO_2(CO_3)_3^{4-}$ and $U(OH)_4(aq)$ calculated by THCC and MCOTAC. The $UO_2(CO_3)_3^{4-}$ profiles show small oscillations left to the pulse shape profile whereas the $U(OH)_4(aq)$-profiles show no oscillations for the THCC calculation.

The comparison of the calculations by THCC and MCOTAC for two solids showed a better conformity for the solid $UO_2(s)$ than in the uranium-iron system. The precipitation fronts are identical and the solid concentrations calculated by MCOTAC are fluctuating around the THCC-produced curves due to the random walk transport approach in the liquid phase (e.g. by fluctuations in the $UO_2(CO_3)_2^{2-}$- concentration). The concentration profiles for the solid $UO_2(OH)_2 \cdot H_2O(s)$ did not agree to the same degree. The zones of precipitation are in the same region but the concentration levels differ by more than one order of magnitude. As for the uranium-iron system, the change of Eh is responsible for the precipitation of the solids. Because first, $UO_2(s)$ precipitates (caused by the main redox system changes) and then afterwards $UO_2(OH)_2 \cdot H_2O(s)$ precipitates, the second solid is more affected by the species concentrations in solution. Its front moves forward and backward with respect to individual grid cells within the MCOTAC calculation. This is caused by the low amount of the solid $UO_2(OH)_2 \cdot H_2O(s)$ and the varying number of particles which can "dissolve" (or precipitate) the whole $UO_2(OH)_2 \cdot H_2O(s)$ amount in a grid cell from one time step to another. Therefore, the $UO_2(OH)_2 \cdot H_2O(s)$ profile calculated by MCOTAC showed the same discrepancies as the $UO_2(s)$-profiles for the uranium-iron redox system in Chapt. 3.2 caused by the randomly varying concentrations of related basis species in the liquid phase.

The fact, that the $H_2(aq)$, HCO_3^- and OH^- profiles are in good agreement underlines, that the differences for the $UO_2(CO_3)_2^{2-}$ or H^+ profile are mostly due to the overshooting of THCC calculations near the front where both solids coexist, and not due to other effects.

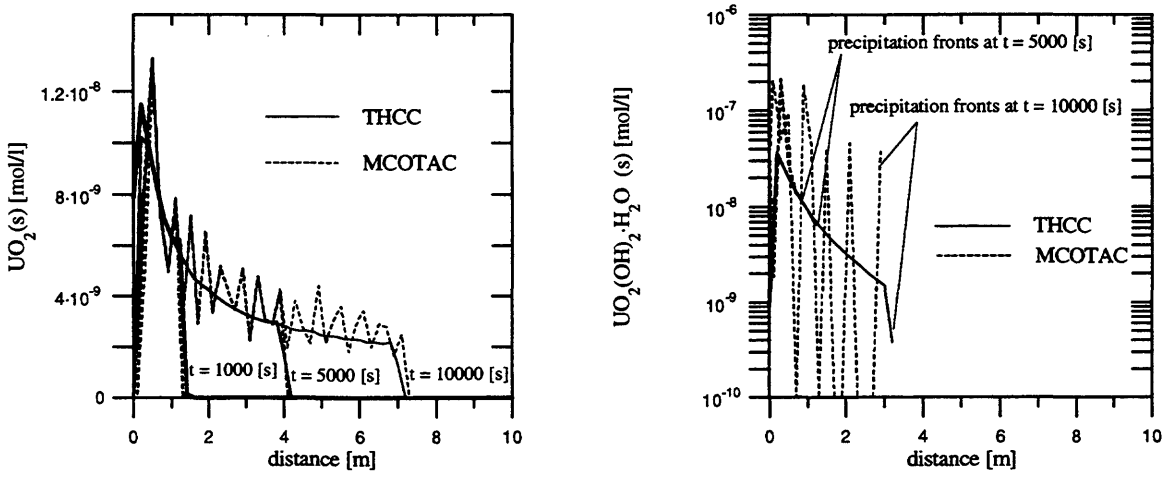

Figure 4.6: Comparison of the concentration profiles of the solids $UO_2(s)$ and $UO_2(OH)_2 \cdot H_2O(s)$ calculated by THCC and MCOTAC.

In addition to the shown concentration profiles and the *Eh-pH* diagram for the condition of coexisting solids $UO_2(s)$ and $UO_2(OH)_2 \cdot H_2O(s)$, Fig. 4.7 shows the chemical system development in form of the master reductant concentration, $H_2(aq)$, with migration time at a fixed location in the column in the *Eh-pH* space. It describes the pathway of the chemical system from initial column conditions to the inlet condition which will be reached after infinite time. It is obvious that first the $H_2(aq)$ concentration decreases fast with increasing *Eh* while the *pH* of the system nearly stays constant. During this period the $U(OH)_4(aq)$ rises up to $4.08 \cdot 10^{-10}$M, after which $UO_2(s)$ precipitates, independent of *Eh* or *pH* as indicated in Eq. (3-3) and accompanying discussion, so the solid $UO_2(s)$ is present at x=1.1 m at a migration time of 1000 s. Then, at about a $\log[H_2(aq)]$ of -19, the *pH* decreases too. The $H_2(aq)$ concentration decreases slowly now with slower increasing of *Eh* and decreasing of *pH* in the direction of the chemical condition of the inlet solution. At a migration time of about 6000 s the solid $UO_2(OH)_2 \cdot H_2O(s)$ precipitates too, because with decreasing *pH* condition (4-5) is fulfilled for the coexistence of the two solids. This figure gives a indication how this redox system develops with time and where or at which time numerical problems may occur.

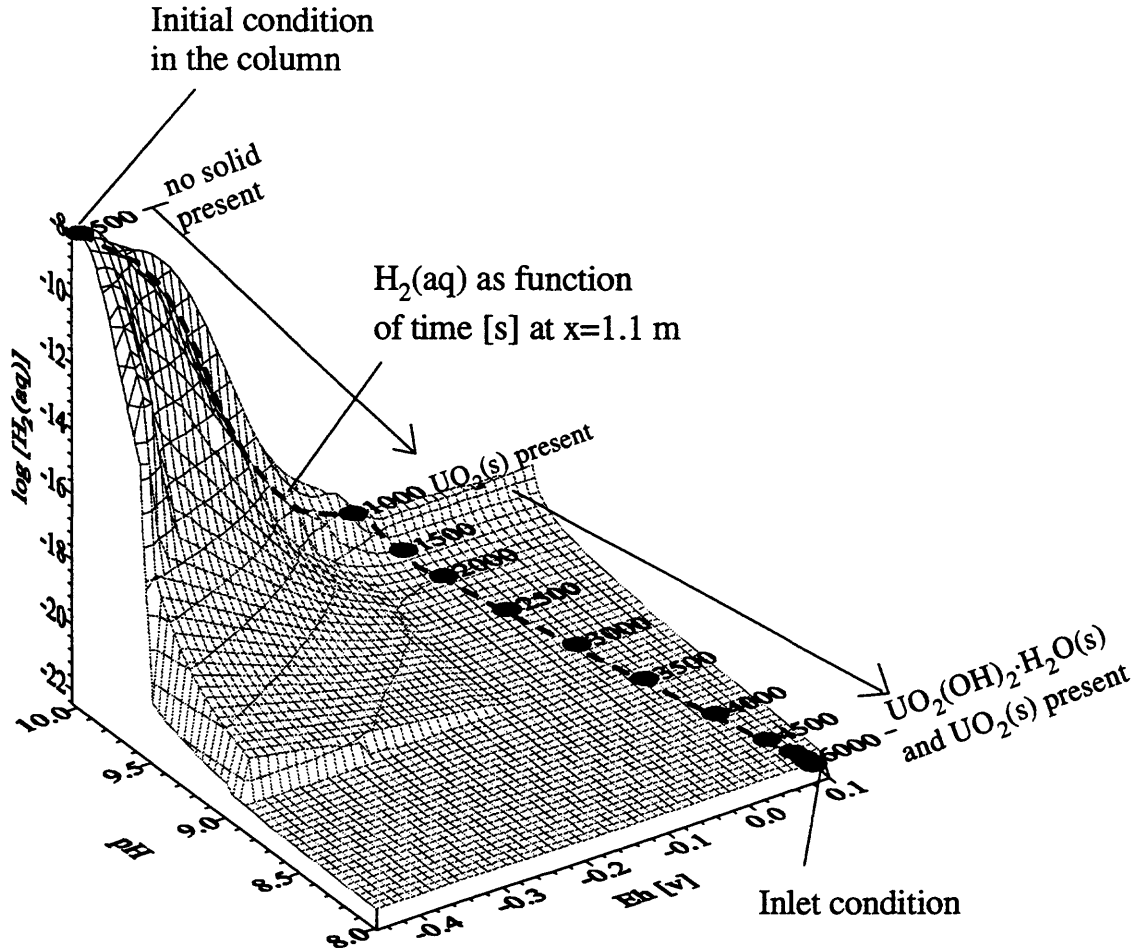

Figure 4.7: Pathway of the redox system in Eh - pH space from initially defined composition to the final (inlet) condition. The surface plot corresponds to a inverse distance to a power of two interpolation of all $H_2(aq)$ concentration (master reductant) in the Eh - pH space calculated for all nodes at 20 different times during a total migration time of 10000 s (the changes from 6000 s to 10000 s at this location are very small).

4.2.2 Influence of basis species set

To investigate the behaviour of the two codes with respect to the oscillations occurring in the aqueous concentration profiles (THCC) or in the solid profiles (MCOTAC) a different set of basis species was used. This set consists of bare ions, whereas the former set consists of master ions present at the highest concentration levels. Instead of $UO_2(CO_3)_2^{2-}$, HCO_3^-, H_2(aq), OH^- and Na^+, now the bare ions UO_2^{2+}, CO_3^{2-} and H^+ are used as basis species. The transport parameters are the same as before. The chemical equilibria with H_2(aq), and Na^+ have to be written in terms of the revised basis species set. Also the inlet and initial conditions have to be recalculated to account for the new basis species set. These conditions

and the comparison of calculated concentration profiles by THCC and MCOTAC are summarised in App. A for completeness. In the following the main results on the dependency of the basis species set is discussed.

With a changed set of basis species, the dissolution of the solids have to be written in terms of the new basis species set (compare Eq. 4-3 and 4-4):

$$UO_2(OH)_2 \cdot H_2O(s) = UO_2^{2+} - 2H^+ + 3H_2O(l),\ \log K_{sp} = 4.83336 \tag{4-8}$$

$$UO_2(s) = UO_2^{2+} - 2H^+ + H_2(aq),\ \log K_{sp} = -16.99290 \tag{4-9}$$

Combining reaction (4-8) with (4-9) produces:

$$UO_2(OH)_2 \cdot H_2O(s) + H_2(aq) = UO_2(s) + 3H_2O(l),$$
$$\log K_{sp} = -\log[H_2(aq)] = 21.82626 \tag{4-10}$$

Then the two solids coexist when $[H_2(aq)] = 1.492 \cdot 10^{-22}$ M which must be equal to the value calculated with the other species set; condition (4-7) is also valid for this system.

A comparison of the calculated profiles is shown in Fig. 4.8 for the species H^+ which is a basis species in one calculation and a complex in the other. In both cases, there is no general improvement of the agreement or a reduction in the oscillating profiles calculated by THCC. Also the random fluctuations are of the same order. The comparison of the other concentration profiles of basis species, complexes and solids show the same tendency.

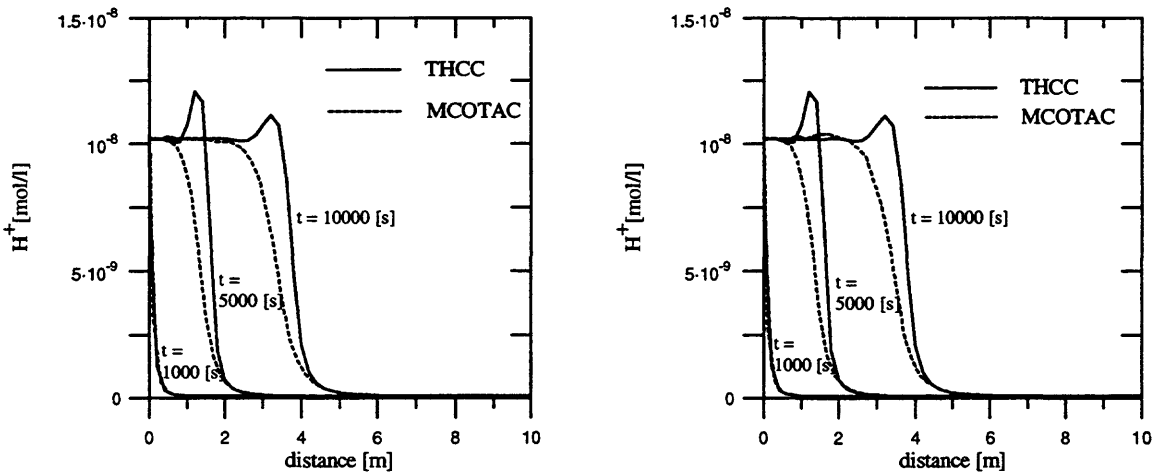

Figure 4.8: Comparison of the concentration profiles calculated for different sets of basis species. On the left H^+ was defined as a complex, on the right it was defined as a basis species.

A different behaviour was observed in relation to the initial system definition. If UO_2^{2+} was used as the uranium bearing basis species, a dummy zero concentration not equal zero has to be used for the initial uranium concentration in the column otherwise numerical problems

occurred for the equilibrium calculation of the initial chemical system in the column. In case of $UO_2(CO_3)_2^{2-}$ as the basis species zero concentration can be used without any numerical problems. A reason could be that in the second case UO_2^{2+} was not taken into account as a complex because it was present at a low concentration level. In addition to this example of a system blowing up, if the basis species set was changed, a better convergence behaviour during the dynamic calculation was observed in some cases but without a general rule for improving convergence behaviour. Using different sets of basis species for calculation can help to find more convergent systems during the dynamic calculation to minimise the total computation time or to get convergence at all[15].

4.2.3 Influence of boundary condition changes

For this simulation the inflowing solution is not saturated with respect to the solid $UO_2(OH)_2 \cdot H_2O(s)$. All other parameters are as defined in 4.2.1. This changes the composition of the inflowing water (see App. B) with the result that the precipitation of this solid is delayed in the column a little, relative to the previous uranium-hydrogen simulations. The solid $UO_2(OH)_2 \cdot H_2O(s)$ does not precipitate at the first node, and the region of precipitation moves away from the influx boundary as simulated time increases.

The calculated concentration profiles of the solutes did not differ significantly from the previous calculations and are shown in App. B for completeness. Only some differences occurred for the solids $UO_2(OH)_2 \cdot H_2O(s)$ and UO_2(s) due to the minor concentration of uranium bearing ions in the inlet solution. Therefore, the solid $UO_2(OH)_2 \cdot H_2O(s)$ precipitated at little later times and then dissolved again. In contrast to former calculations, where no $UO_2(OH)_2 \cdot H_2O(s)$ dissolution occurred due to the saturation of the inlet solution with respect to $UO_2(OH)_2 \cdot H_2O(s)$, here, two precipitation and dissolution fronts of $UO_2(OH)_2 \cdot H_2O(s)$ and UO_2(s) moved through the column. The chemical system and its chemical development did not change significantly in the domain but the temporal scale of the chemical development in the domain changes due to another inlet solution. The $UO_2(OH)_2 \cdot H_2O(s)$ and UO_2(s) profiles are calculated at a little lower level due to the temporal retardation (see Fig. 4.9), and in the final chemical system there would be no solid in the domain.

Depending on the choice of basis species set THCC calculations gave different results with respect to the solid $UO_2(OH)_2 \cdot H_2O(s)$. For calculations with the major ions used as basis species set, the solid $UO_2(OH)_2 \cdot H_2O(s)$ precipitates and afterwards dissolves at successive nodes within a short time, so that there was no solid $UO_2(OH)_2 \cdot H_2O(s)$ present along the whole column for most of the calculated migration time[16]. Hence, for THCC calculations

---

[15]Within the next system calculation with slightly changed boundary (inlet) conditions another example was given for the influence of the choice of basis species set. Depending on the chosen set, there a different precipitation and dissolution behaviour of a solid was observed for the THCC calculations.

[16]The solid $UO_2(OH)_2 \cdot H_2O(s)$ was not present in the spatial domain at t = 5000 s and t = 10000 s for THCC calculations with the major ions basis species set. The solid was calculated present only for a few tens of seconds at a given node before it dissolved again.

with the bare ions used as basis species set, $UO_2(OH)_2 \cdot H_2O(s)$ shows a precipitation and dissolution front moving through the column which correspond to the MCOTAC calculated ones[17]. The precipitation fronts of $UO_2(OH)_2 \cdot H_2O(s)$ at 5000 s were at 0.5 m (MCOTAC) and at 1.2 m (THCC), and the dissolution fronts at 0.0 m (MCOTAC) and at 0.2 m (THCC). This means that the THCC calculated fronts moved a little further into the domain than those calculated by MCOTAC. Also at 10000 s the dissolution fronts were further from the inlet for THCC than for MCOTAC calculations.

These redox example calculations show that depending on the set of basis species, different numerical calculations lead to a different appearance of precipitation and dissolution fronts for the solid $UO_2(OH)_2 \cdot H_2O(s)$ just precipitating above saturation with respect to the chosen chemical description of the system[18]. Another reason for the differences in the precipitation and dissolution fronts, apart from the difficulties within MCOTAC for solids just above saturation, could be the "dummy" initial concentration of the basis species UO_2^{2+} of $1 \cdot 10^{-20} [mol / l]$ in the spatial domain. This was used in connection with the bare ion basis species set to overcome convergence problems within the static initial chemical equilibrium calculation for both codes (see Chapt. 4.2.2).

---

[17]These calculated profiles are more reliable because they were calculated by two different codes more or less the same, whereas THCC calculation with the major ions basis set could not be reproduced by MCOTAC calculations.

[18] The basis species set of major ions includes $UO_2(CO_3)_2^{2-}$ as a basis species but it did not include UO_2^{2+} as a complex, whereas the basis species set of bare ions includes UO_2^{2+} as a basis species and $UO_2(CO_3)_2^{2-}$ as a complex, too.

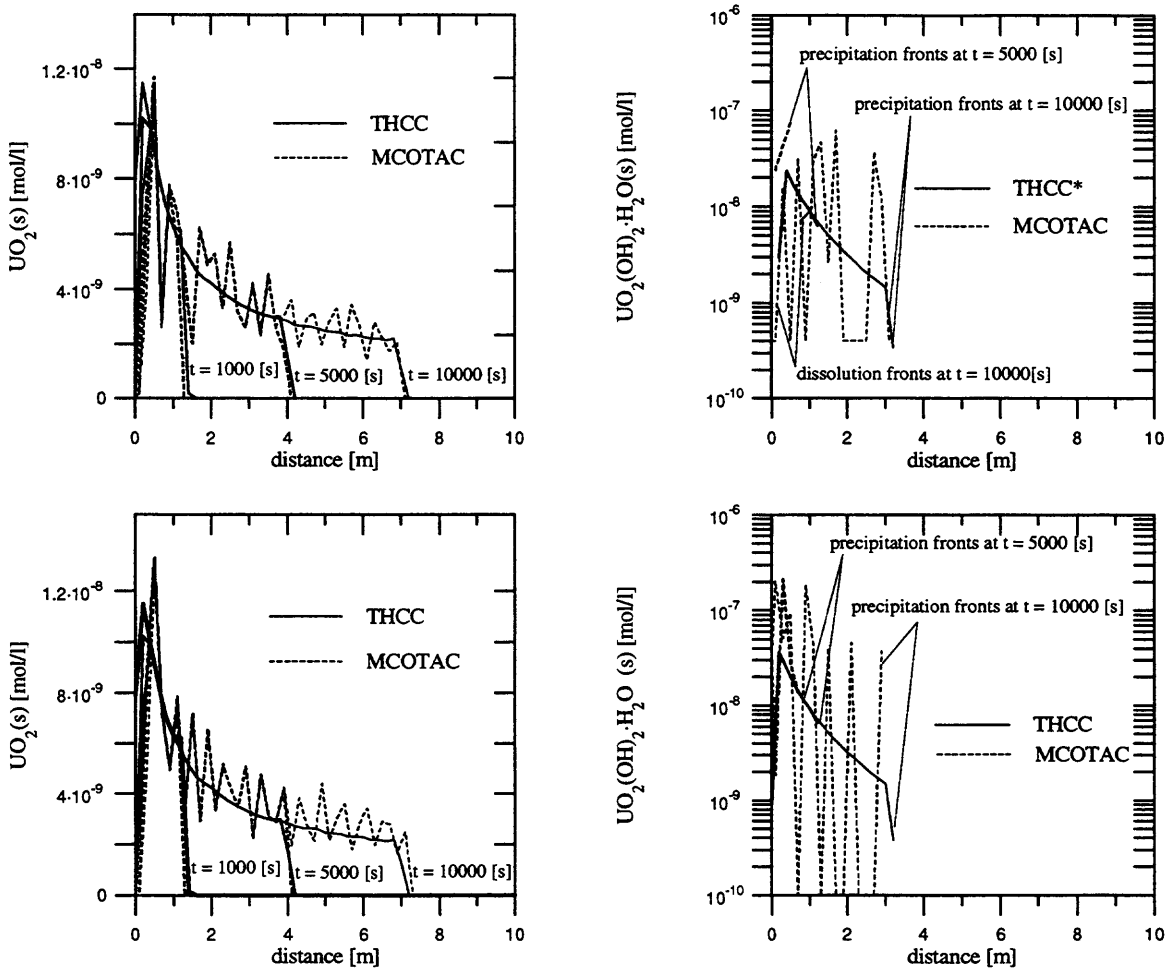

Figure 4.9: Comparison of concentration profiles of the solids $UO_2(s)$ and $UO_2(OH)_2 \cdot H_2O(s)$ calculated for two different inlet boundary conditions (as defined for 4.2.1 at bottom, as defined for 4.2.3 on top). In the case of THCC calculations with major ions used as basis species set, the $UO_2(OH)_2 \cdot H_2O(s)$ precipitation and dissolution fronts were close together at early times (at nodes <6), and solid precipitation vanished completely at later times. For THCC calculations with bare ions used as basis set $UO_2(OH)_2 \cdot H_2O(s)$ precipitation and dissolution front moved through the column. For MCOTAC calculations a 'switching' between 'solid' and 'no solid' occurred for neighbouring nodes within the same spatial domain. This behaviour was more pregnant for the solid $UO_2(OH)_2 \cdot H_2O(s)$ than for $UO_2(s)$ which precipitates first in the temporal system development at a certain location (see Fig. 4.7).*

4.2.4 Influence of spatial grid size

For this comparison the same chemical system is used as in 4.2.1. The transport parameters are also the same, except that now the column length was chosen to be 20 m with a grid size of 0.4 m. This results in a more coarse spatial grid than for all previous calculations. The simulated migration time is 15000 s to allow a migration further into the column. The conformity of THCC and MCOTAC calculations is the same as for comparisons above. No significant differences occurred in the concentration profiles for the basis species $UO_2(CO_3)_2^{2-}$, HCO_3^-, H_2(aq) and OH^- (see App. C). Only small oscillations occurred in the $UO_2(CO_3)_2^{2-}$, HCO_3^- and OH^- profiles calculated by THCC, always left of the $UO_2(OH)_2 \cdot H_2O(s)$ precipitation front. The same is true for the complex species e.g. $UO_2(CO_3)_3^{4-}$, except for the H^+ profile where the oscillation in the THCC concentration profile exceeds 200% deviation from the inlet level (Fig. 4.10).

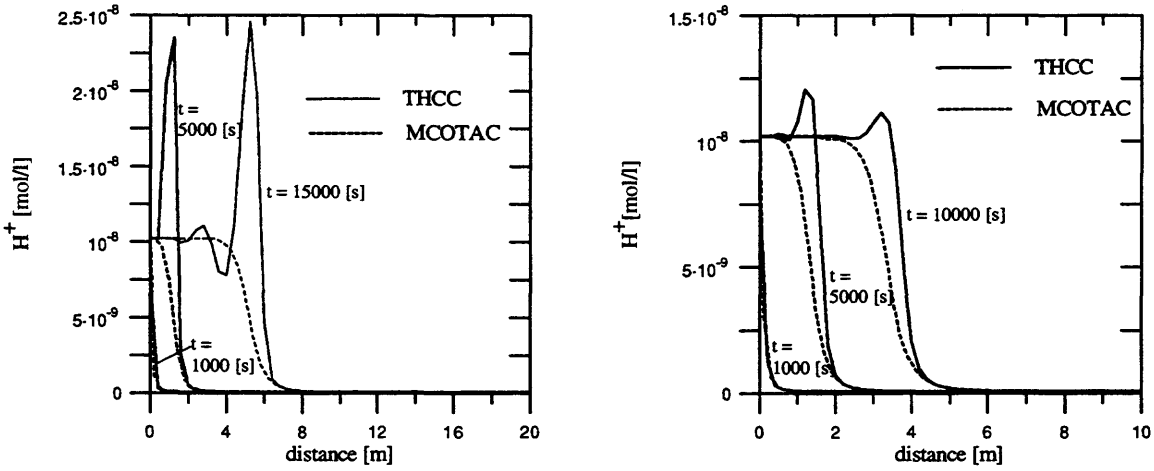

Figure 4.10: Influence of spatial grid size on the concentration profiles of the complex H^+ calculated by THCC and MCOTAC: 0.4 m (left) and 0.2 m (right). (Different scales and times!)

This growing oscillation is only related to the increasing of the grid size compared to calculations in 4.2.1 because all other parameters remained constant. Additionally, the oscillation in the profile was increasing with migration time as a comparison of the H^+ profile at 5000 s and 15000 s shows. This is in contrast to previous THCC calculations. There the oscillations within the profiles decrease with migration time. Such increasing oscillations in the calculated concentration profiles indicate convergence problems, and can lead to a general divergence within the directly coupled code calculations.

A coarser grid was used for the MCOTAC calculations, if only the first ten meters of the column are looked at. Compared to previous MCOTAC calculations a lower number of particles was used because only one half of this column corresponds to former calculations with a column length of 10 m. This should lead to larger random fluctuations in calculated concentration profiles. But the decrease of a factor two of number of particles per cell did

not show a corresponding increase in the variation in the calculated profiles by MCOTAC (Fig. 4.10 and 4.11).

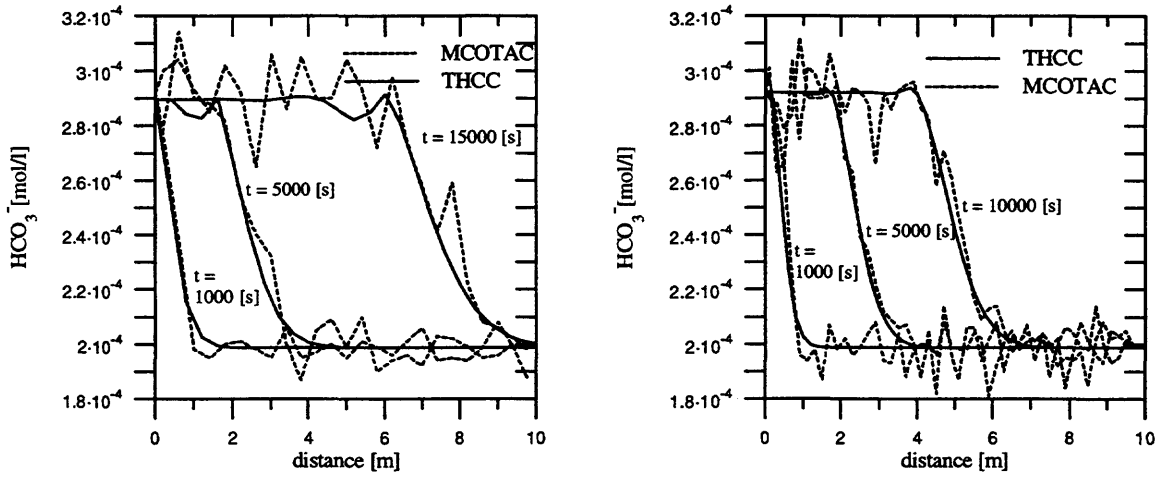

Figure 4.11: Influence of spatial grid size on the concentration profiles of the basis species HCO_3^- calculated by THCC and MCOTAC. For a grid size of 0.2 m 30000 particles are used within MCOTAC calculations (right); and for a grid size of 0.4 m 15000 particles are used within MCOTAC calculations (left) for a column length of 10 m in each case.

Although, for THCC calculations the overshooting behaviour increased dramatically for the H^+ profile (Fig. 4.10) and started already for the HCO_3^- profile (Fig. 4.11) the calculated solid concentration profiles showed no additional changes compared to profiles calculated in Chapters 4.2.1 and 4.2.2 besides the fact that the location of the solid precipitation fronts were slightly further within the domain for calculations with the coarse grid for t = 1000 s and t = 5000 s than those with the fine grid (see App. C) which could be explained by a lower spatial resolution for this calculation.

The influence of the chosen grid size on the oscillation within the concentration profiles calculated by THCC needs further investigation because of its possible influence on the general convergence for THCC calculations. As shown in Chapt. 3.2, increasing the dispersion length while holding all other parameters constant causes a decreasing oscillation of the concentration profiles calculated by THCC. By increasing the dispersion length the concentration fronts become smoother but the modelled system changes to more dispersive transport. Instead of changing a system parameter (dispersion length) a 'description' parameter like the grid size can be changed as well to decrease the observed oscillations in the concentration profiles. An example for the effect of a varying grid size was already given. In addition to that a further calculation with 101 nodes and a grid size of 0.1 m was done to reduce occurring oscillating concentration profiles for THCC calculations (Fig. 4.12). To suppress oscillations within a pure advective dispersive transport description by

finite difference methods[19] a criterion was proposed for the (grid) Peclet number *Pe* [Kinzelbach, 1987], defined by:

$$Pe = \left| \frac{\Delta x \cdot v}{D} \right| \leq 2 \qquad (4\text{-}10)$$

where Δx is the grid size, v the flow velocity and D the dispersivity. Applying the criterion in this case shows that the grid size of 0.4 m is related to a Peclet number of 8, a grid size of 0.2 m to a Peclet number of 4 and a grid size of 0.1m to a Peclet number of 2. Only with the last grid size condition (4-10) is fulfilled, but this condition was given only for purely advective-dispersive transport. The oscillating behaviour was also influenced by the choice of the basis species as shown in Chapt. 4.2.2 where the oscillations in the uranium bearing basis species profile was about 35% compared to <5% for the uranium bearing basis species profile in Chapt. 4.2.1. Source or sink terms for species concentrations in heterogeneous systems described here are also not included for the derivation of Eq. (4-10). Further, those oscillations, occurring e.g. for a Peclet number of 4, are only present for a few species in a calculation and are not a general feature of all species (although the transport parameters were equal for all species in solution), so that this criterion can not be applied. Within the dynamic calculations these oscillations can force the numerical system to 'blow up' (no convergence). Criteria such as (4-10) to set up a mathematical description for this type of a coupled system do not exist. Therefore, the calculation should be checked by several slightly different system calculations, by comparison of different code applications or by different types of system description (different sets of basis species) which should give plausible and consistent results.

[19] Within THCC a finite difference formulation for the transport description is used.

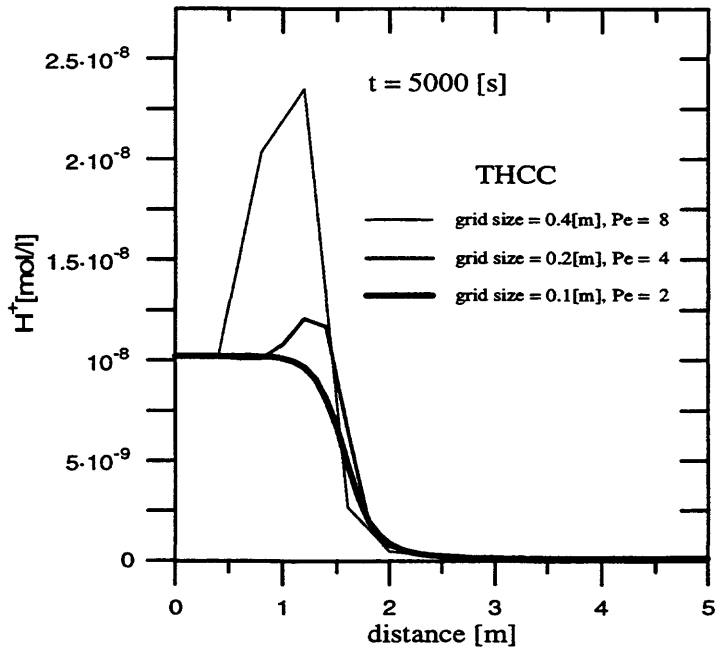

Figure 4.12: Oscillations in the H^+ concentration profile as function of grid size, and related the Peclet number Pe, for THCC calculations.

4.2.5 Used CPU time for the uranium-hydrogen redox system for THCC and MCOTAC calculations

From Tab. 4.10 it can be seen that the calculation of the real time systems of about 8000 s to 15000 s takes about 100 s calculation time which is just a factor of 100 less. But the coupled systems are quite complex and numerically difficult so that a transfer to other systems will be not realistic if the CPU time is concerned. The given ranges of CPU time are results of parameter changes. In case of MCOTAC calculations the number of used particles for the transport description influences the CPU time. Also the amount of output data produced is a factor for these example calculations because much output was produced for comparison of the calculations for a relative short migration time. Further it can be seen that calculations on the Titan-computer are up to four times faster than on the i860 inboard. Not included in this table are the CPU times for calculations which 'blow up'. In some cases a calculation on the i860 gave plausible results whereas on the Titan the same calculation showed no convergence. These problems occurred mostly within the numerical iteration process calculating chemical equilibria in a dynamic system. Therefore a further investigation or improvement is necessary for the future.

Table 4.10: Used CPU time for uranium hydrogen redox calculations for THCC and MCOTAC on different hardware systems (blank cells: no calculation done)[20]

		CPU time[21] in [s] used for the uranium hydrogen systems			
Model	Hardware	4.2.1	4.2.2	4.2.3	4.2.4
THCC	i860[22]	258		605	
	titan[23]	140	214	150	157
MCOTAC	i860	221	114 - 121	76 - 138	121
	titan	80 - 114			

5. Conclusion and recommendations

The comparison of calculation of redox reactions in groundwater flow systems by two different coupled codes showed a good agreement for the calculated concentration profiles. The numerically difficult systems with high concentration gradients are handled well by both codes. The forms and locations of the redox fronts coincide. The concentration profiles of species in the liquid phase were calculated in general only with small differences for the uranium-iron redox system and for the uranium-hydrogen redox systems, and agree well when different sets of basis species were used for the chemical system description. Differences occurred for some species in combination with the solid precipitation fronts.

For a few species THCC calculations gave oscillating concentration profiles near the precipitation front, which were also influenced by the choice of the set of basis species used for description. These oscillating concentration profiles did not occur for MCOTAC calculations. For THCC calculations these oscillations can be reduced by reducing the grid size in the given system in order to decrease the grid Peclet number and to fulfil a convergence criterion defined for pure advective dispersive transport. This indicates that the origin of the occurring oscillations in the concentration profiles are related to the finite difference formulation used within THCC for transport description but a general criterion for coupled transport and chemical equilibrium chemistry cannot be deduced from the pure

---

[20] The comparison of example calculations on different hardware systems is not complete but allow a comparison of used CPU-time on different hardware for the two codes.

[21] CPU - time ≡ turn around time for a single user application.

[22] Intel i860 inboard (40MHz) within a '486 PC (33MHz).

[23] Kubota Stardent 3020 (2 processor UNIX graphics workstation).

transport criterion to overcome these difficulties within the directly coupled code applications.

MCOTAC calculations of the solid concentration profiles gave less satisfactory agreement for the solids $UO_2(s)$ and $UO_2(OH)_2 \cdot H_2O(s)$ if the calculated amount of the solid was compared. $UO_2(s)$ in the uranium-iron redox system (Chapt. 3.2) and $UO_2(OH)_2 \cdot H_2O(s)$ in the uranium-hydrogen systems (Chapt. 4.2) were calculated by MCOTAC up to higher levels for some nodes and at the same time zero amount (no solid) at several intermediate nodes. This can be explained by the fact that concentrations of these solids were strongly influenced by the concentrations of $U(OH)_4(aq)$ (influence $UO_2(s)$ in Chapt. 3.2) and $H_2(aq)$ (influence $UO_2(OH)_2 \cdot H_2O(s)$ in Chapt. 4.2) which were varying within the random walk description of transport by MCOTAC. For these example calculations the amount of precipitated solid cannot act as a buffer for species concentration in solution because the amount of precipitated solid was in the same order compared to the amount of solid forming species in the solution. MCOTAC-calculated profiles of $UO_2(s)$ in the uranium-hydrogen redox system (Chapt. 4.2) varied more closely around the THCC-calculated profiles than those for $UO_2(s)$ in Chapt. 3.2 or $UO_2(OH)_2 \cdot H_2O(s)$ in Chapt. 4.2. In this case two solids were present which precipitated subsequently, and the concentration of $UO_2(s)$ seems not to be as directly influenced by variations of aqueous species' concentrations as in the case of $UO_2(OH)_2 \cdot H_2O(s)$.

Comparison of the used CPU times for both coupled codes showed a shorter runtime for the MCOTAC calculations (up to a factor of six for the uranium-iron system Chapt. 3). The calculation times can grow indefinitely if the chemical equilibrium calculations do not converge for some chemical system set-up's. This behaviour can be observed for both codes and an improvement in the chemical equilibrium calculations in future is desirable, e.g., by application of different iteration procedures.

MCOTAC calculations of heterogeneous redox systems showed that the application of a sequentially coupled code gives results, in general, comparable to those produced by a directly coupled code. An advantage of the MCOTAC method can be the shorter runtime for the calculations and non-oscillatory species concentration profiles in the liquid phase. Oscillatory behaviour arises in the directly coupled code THCC due to the finite difference formulation but a general definition of a convergence criterion to exclude such a behaviour seems not to be possible. In chemical systems where the liquid phase is saturated with respect to the solid and the solid is present at very low concentration, MCOTAC calculations show a "switching" behaviour between solid-present and solid-not-present at neighbouring cells. This behaviour should be kept in mind for future simulations of solids in real geochemical systems.

The application of two different codes helps to produce a more reliable description of coupled systems if no analytical solutions are present and allows reliable predictions. Further, these exercises showed that the defined systems, which are numerically difficult, can be handled by such codes with advantages or disadvantages for the individual code. The application of MCOTAC to perhaps more complex or real but less numerically difficult geochemical systems should be possible as well because the CPU time, as an indicator of the applicability of a code, was reduced up to a factor of six compared to THCC applications presented here.

Acknowledgements

We would like to thank all colleagues at PSI contributing to this work by comments and discussions during the preparation. Special thanks go to Drs. J. Hadermann and U. Berner for their fruitful and constructive discussions during the development of this report, to Dr. V. Pot for the translation of the abstract and to Dr. Ph. Jamet for his criticisms and comments on the manuscript.

Partial financial support by the Swiss National Cooperative for the Storage of Radioactive Wastes, NAGRA, is gratefully acknowledged.

References

Carnahan, C.L. (1986): Simulation of Uranium Transport with Variable Temperature and Oxidation Potential: The Computer Code THCC, in Mat. Res. Soc. Symp. Proc. ***84:*** *MRS, Pittsburgh, Pa. p. 713-721.*

Carnahan, C.L. (1988): Some Effects of Data Base Variations on Numerical Simulations of Uranium Migration. *Radiochemica Acta,* ***44/45:*** *p. 349-354.*

Gresho, P.M. and R.L. Lee (1981): Don't suppress the wiggles - they're telling you something. *Computers and Fluids,* ***9:*** *p. 223-253.*

Kinzelbach, W. (1987): Numerische Methoden zur Modellierung des Transports von Schadstoffen im Grundwasser. *Schriftenreihe gwf Wasser - Abwasser,* ***21:*** *p. 211ff.*

Pfingsten, W. (1994): Modular Coupling of Transport and Chemistry: Theory and Model Applications. *Paul Scherrer Institut, PSI-Bericht* ***94-15*** *and NTB* ***94-19.***

Prickett, T.A., T. Naymik and G. Lonnquist (1982): A 'Random-Walk' Solute Transport Model for Selected Groundwater Quality Evaluations. *Illinois State Water Survey, Bulletin* **65**.

Stumm, W. and J.J. Morgan (1981): Aquatic Chemistry. *John Wiley & Sons, Inc., New York*

Appendix

Within the appendix a more complete description of the modelled chemical systems and a further comparison between concentration profiles calculated by THCC and MCOTAC are given. The appendices are divided with respect to the different systems modelled.

Appendix A: Summarised system description and calculation results related to Chapter 4.2.2 - Influence of changing basis species set

Using bare ions as basis species for the uranium-hydrogen system the chemical equilibrium and initial conditions have to be rewritten in terms of this set of basis species (Tab. A.1). The inlet solution is saturated in respect to the solid $UO_2(OH)_2 \cdot H_2O(s)$, the column length is 10 m (grid size is 0.2 m) and the simulated migration time is 10000 s, same as in 4.2.1.

Table A.1: Chemical reactions and equilibrium constants (at 25° C) used with bare ions as basis species set (see footnote 1).

reactions used in combination with bare ions as basis species	logK
$H_2O(l)$ - $H^+ = OH^-$	-13.9954
$CO_3^{2-} + H^+ = HCO_3^-$	10.3288
$CO_3^{2-} + 2H^+ - H_2O(l) = CO_2(aq)$	16.6737
$UO_2^{2+} - H^+ + H_2O(l) = UO_2OH^+$	-5.20827
$UO_2^{2+} + CO_3^{2-} = UO_2CO_3\ (aq)$	9.61470
$UO_2^{2+} + 2CO_3^{2-} = UO_2(CO_3)_2^{2-}$	16.9698
$UO_2^{2+} + 3CO_3^{2-} = UO_2(CO_3)_3^{4-}$	21.5845
$UO_2^{2+} - 2H^+ + 2H_2O(l) + H_2(aq) = U(OH)_4\ (aq)$	7.60349
$UO_2(OH)_2 \cdot H_2O\ (s) = UO_2^{2+} - 2H^+ + 3H_2O(l)$	4.83336
$UO_2\ (s) = UO_2^{2+} - 2H^+ + H_2\ (aq)$	-16.9929

The basis species concentrations of the inlet solution and the initial concentration are given in the following tables[24]:

---

[24] The basis species UO_2^{2+} used here for description of the chemical system was not taken into account as a complex in combination with basis species used in 4.2.1 (major ions used as basis species set) because of its low concentration level. There it was not necessary to include complexes with vanishing contribution to the mass balance.

Table A.2: Inlet concentrations of basis species in solution and amount of solid used to specify the inlet solution[25]. (The amount of solid is given for completeness to allow comparison to codes using total basis species concentration.)

Basis species and solids	total aqueous concentration [mol/l]	species concentration [mol/l]
UO_2^{2+}	$1.3451 \cdot 10^{-6}$	$7.3558 \cdot 10^{-12}$
CO_3^{2-}	$3.0000 \cdot 10^{-4}$	$1.4408 \cdot 10^{-6}$
$H_2(aq)$	$8.9686 \cdot 10^{-11}$	$3.2800 \cdot 10^{-23}$
H^+	$3.0108 \cdot 10^{-4}$	$1.0190 \cdot 10^{-8}$
Na^+	$2.9623 \cdot 10^{-4}$	$2.9623 \cdot 10^{-4}$
$UO_2(OH)_2 \cdot H_2O(s)$	present at $5.4952 \cdot 10^{-8}$	-
$UO_2(s)$	-	-

Table A.3: Initial concentrations of basis species in solution and amount of solid in the spatial domain[26] (see footnote 1).

Basis species and solids	total aqueous concentration [mol/l]	species concentration [mol/l]
UO_2^{2+}	$1.0000 \cdot 10^{-20}$	$2.1574 \cdot 10^{-40}$
CO_3^{2-}	$3.0000 \cdot 10^{-4}$	$1.0127 \cdot 10^{-4}$
$H_2(aq)$	$1.2870 \cdot 10^{-8}$	$1.2870 \cdot 10^{-8}$
H^+	$9.4805 \cdot 10^{-5}$	$1.0270 \cdot 10^{-10}$
Na^+	$5.0519 \cdot 10^{-4}$	$5.0519 \cdot 10^{-4}$
$UO_2(OH)_2 \cdot H_2O(s)$	0	-
$UO_2(s)$	0	-

[25] The chemical system modelled here (Tables A.2 and A.3) is slightly different from the one defined in 4.2.1, because there UO_2^{2+} was not taken into account at all (whether as a complex nor a basis species). This leads to small differences in the inlet and initial species concentrations (see also footnotes 1 and 23).

[26] Here a finite 'dummy' concentration, low but not zero, was used to avoid numerical problems at zero basis species concentration of UO_2^{2+}

The comparison of model calculations with THCC and MCOTAC gives a slightly different behaviour. The general agreement of the calculated profiles is good (Figures A.1 to A.6). Now the uranium-bearing basis species showed an oscillating form for the THCC calculation (Fig. A.1), in contrast to the uranium-bearing basis species $UO_2(CO_3)_2^{2-}$ in Chapt. 4.2.1 (Fig. 4.2). The profiles of the solids were similar to those in Chapt. 4.2.1. The concentration profiles of the species in solution in Chapt. 4.2.1 are reproduced in Chapt. 4.2.2, independent of the type (complex or basis) of species[27]. Only the degree of the overshooting behaviour within the THCC calculations changed slightly by using another set of basis species. Differences in MCOTAC calculations for both sets of basis species did not occur. The reason that no identical profiles were calculated, e.g., for the $UO_2(CO_3)_3^{4-}$ (Figures 4.5 and A.5) or H^+ (Fig. 4.8) profiles, is the random walk description of the transport within MCOTAC accompanied by random fluctuations of the concentration profiles, and related, the precipitation fronts were moving forth and back with time. The following Figures show the calculated concentration profiles for basis species, complexes and solids with the bare ions used as the basis species set. This allows a more complete comparison to those calculated with the major ions used as basis species set (Chapt. 4.2.1).

.

[27] Change of species type for OH^- (basis species in Chapt. 4.2.1, complex in Chapt. 4.2.2), H^+ (basis species in Chapt. 4.2.2, complex in Chapt. 4.2.1) or $UO_2(CO_3)_2^{2-}$ (basis species in Chapt. 4.2.1, complex in Chapt. 4.2.2)

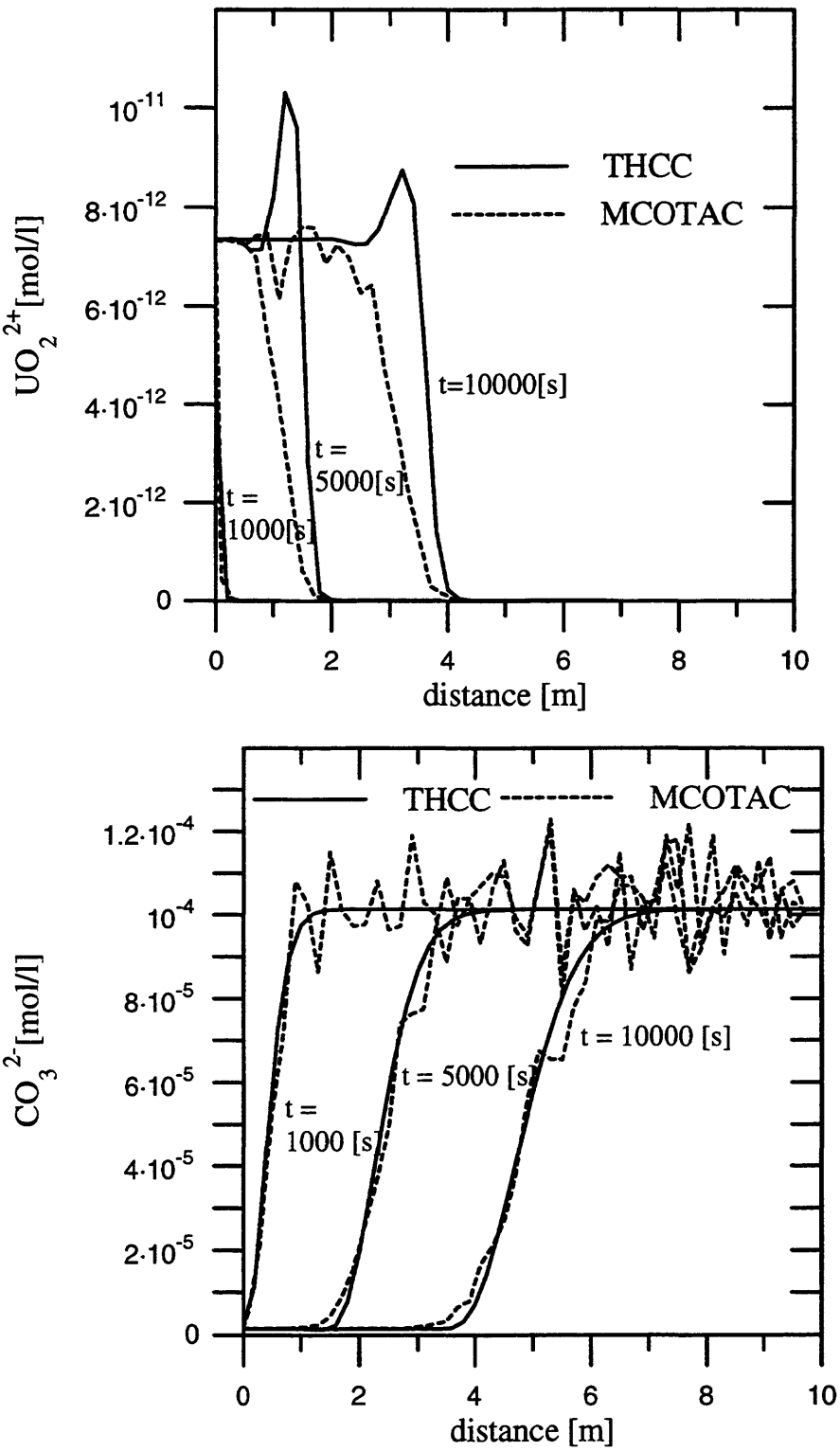

Figure A.1: Comparison of concentration profiles for basis species UO_2^{2+} and CO_3^{2-} calculated by THCC and MCOTAC for different migration times. The UO_2^{2+} profiles show oscillation for the THCC calculation.

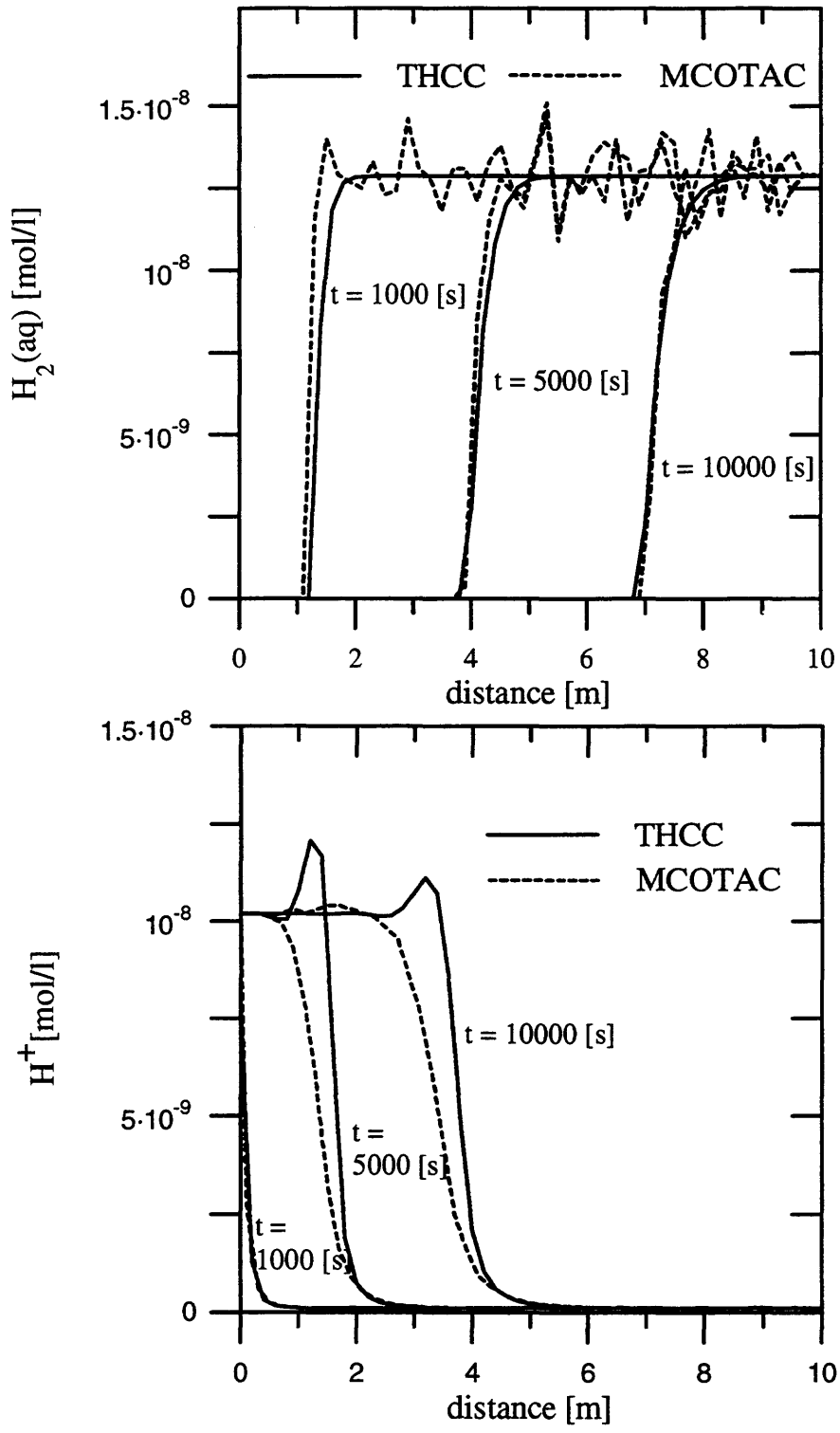

Figure A.2: Comparison of concentration profiles for basis species $H_2(aq)$ and H^+ calculated by THCC and MCOTAC for different migration times. The H^+ profiles show oscillations for the THCC calculation.

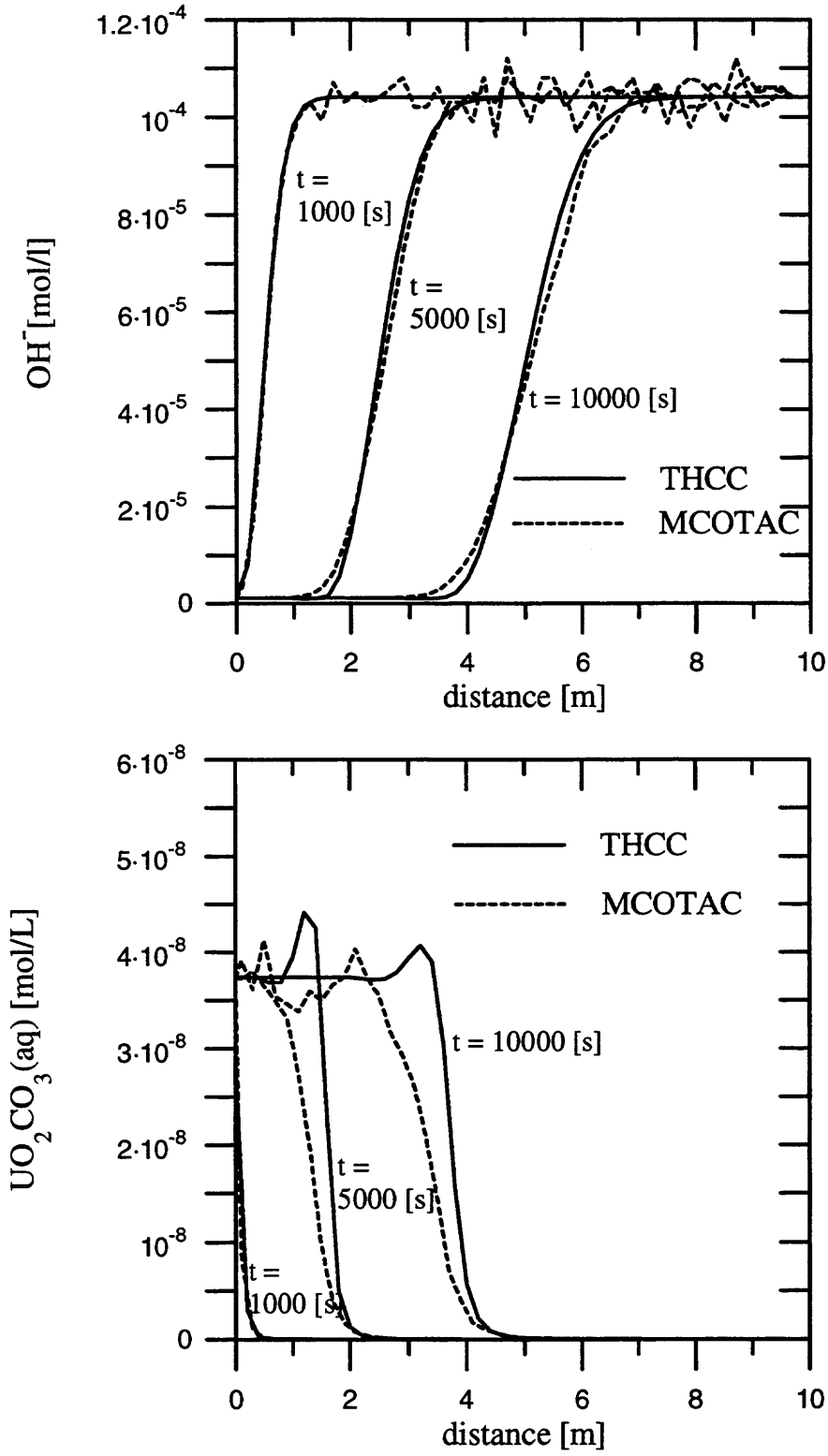

Figure A.3: Comparison of concentration profiles of complex species OH^- and $UO_2CO_3(aq)$ calculated by THCC and MCOTAC for different migration times. The $UO_2CO_3(aq)$ profiles show oscillation for the THCC calculation.

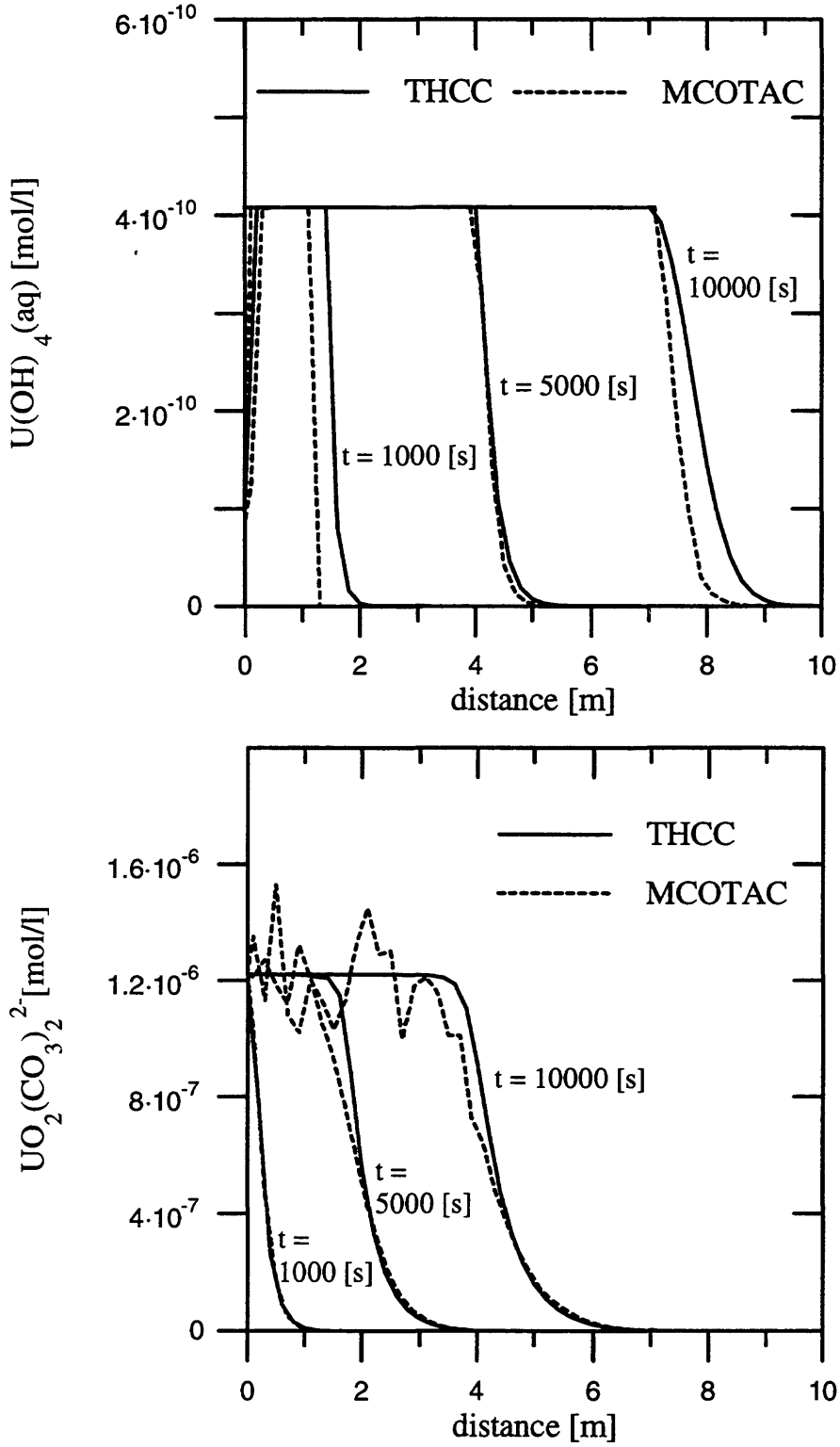

Figure A.4: Comparison of concentration profiles of complex species $UO_2(CO_3)_2^{2-}$ and $U(OH)_4(aq)$ calculated by THCC and MCOTAC for different migration times. The $UO_2(CO_3)_2^{2-}$-profiles and the $U(OH)_4(aq)$-profiles show no oscillation for the THCC calculation (same as in 4.2.1).

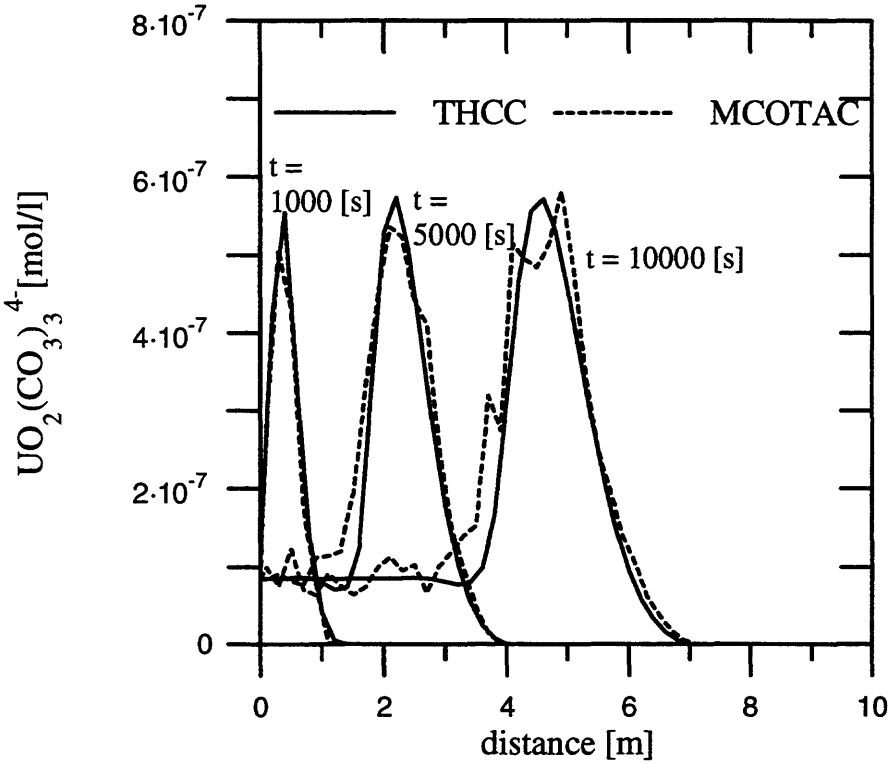

Figure A.5: Comparison of concentration profiles of complex species $UO_2(CO_3)_3^{4-}$ calculated by THCC and MCOTAC for different migration times. The $UO_2(CO_3)_3^{4-}$ profiles show small oscillations left to the pulse profiles for the THCC calculation (same as in 4.2.1).

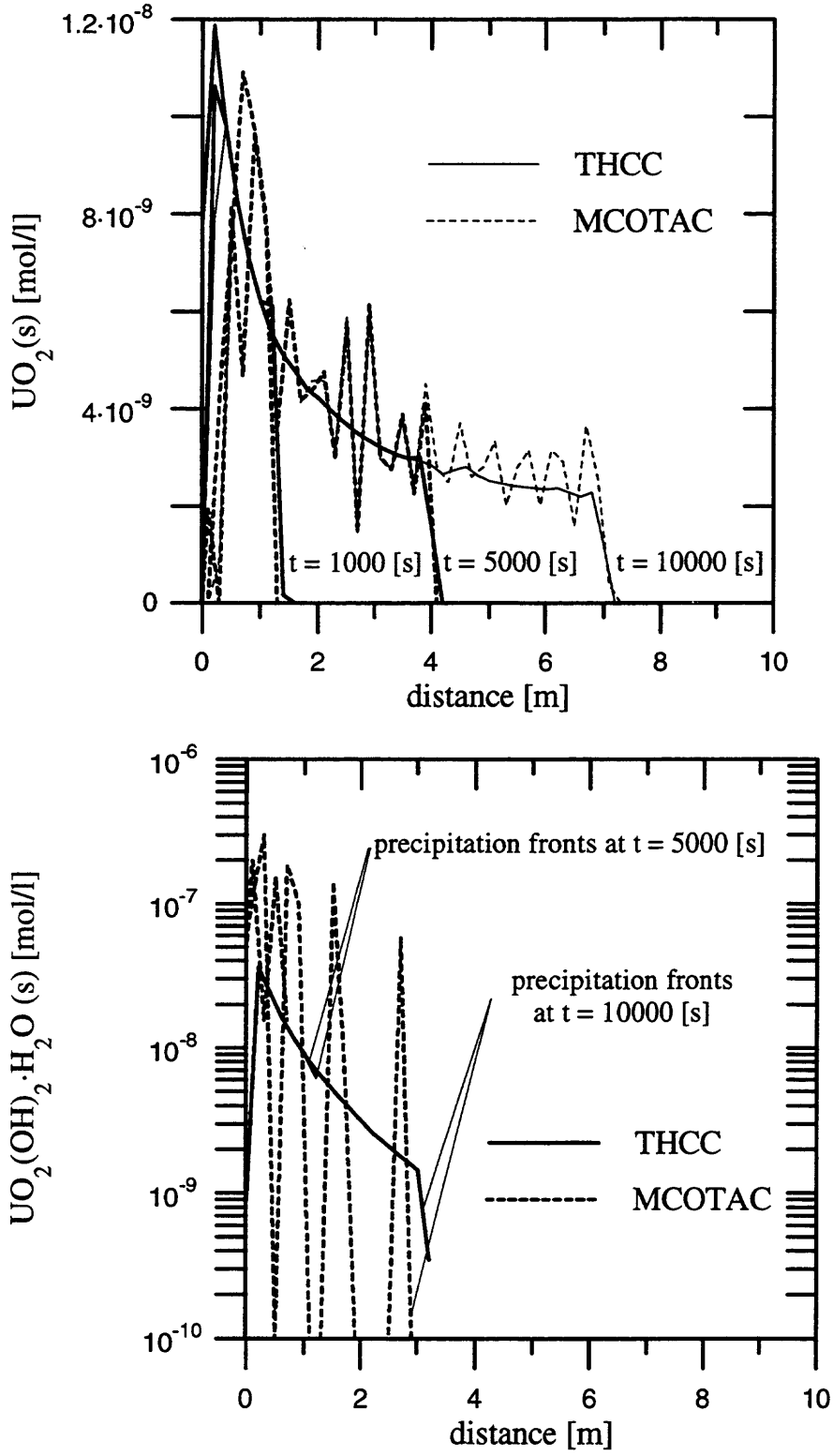

Figure A.6: Comparison of concentration profiles of the solids $UO_2(s)$ and $UO_2(OH)_2 \cdot H_2O(s)$ calculated by THCC and MCOTAC for different migration times.

Appendix B: Summarised system description and calculation results related to Chapter 4.2.3 - Influence of changing boundary conditions

The set of basis species for description of the chemical system, the initial conditions in the column, and the transport parameters are the same as defined in 4.2.1. Only the composition of the inlet solution was changed. It is given in the following table:

Table B.1: Inlet concentration of basis species in solution and amount of solid used to specify the inlet solution (see footnote 1).

Basis species and solids	total aqueous concentration [mol/l]	species concentration [mol/l]
$UO_2(CO_3)_2^{2-}$	$1.3400 \cdot 10^{-6}$	$1.2139 \cdot 10^{-6}$
HCO_3^-	$3.0000 \cdot 10^{-4}$	$2.9217 \cdot 10^{-4}$
H_2(aq)	$8.7675 \cdot 10^{-11}$	$3.2800 \cdot 10^{-23}$
OH^-	$-3.8168 \cdot 10^{-6}$	$1.0310 \cdot 10^{-6}$
Na^+	$2.9886 \cdot 10^{-4}$	$2.9886 \cdot 10^{-4}$
$UO_2(OH)_2 \cdot H_2O(s)$	0	-
UO_2(s)	0	-

The following figures give a more complete comparison of the calculations done with THCC and MCOTAC for this system set up than shown in Chapt. 4.2.3. They show oscillating concentration profiles for THCC calculation of $UO_2(CO_3)_2^{2-}$, HCO_3^- and $UO_2(CO_3)_3^{4-}$ on a low level, H^+ and $UO_2CO_3(aq)$ on a higher level, and no oscillation in the profiles of H_2(aq) (on a linear and a logarithmic scale) and $U(OH)_4(aq)$. The MCOTAC calculated profiles show the known 'zigzag' profiles in good agreement to the THCC calculations.

The differences occurring for THCC and MCOTAC calculations with respect to the solid $UO_2(OH)_2 \cdot H_2O(s)$ and the chosen set of basis species are discussed in Chapt. 4.2.3. For THCC calculations with major ions used as basis species set, the $UO_2(OH)_2 \cdot H_2O(s)$ precipitation and dissolution fronts are close together at early times (at nodes <6). This solid vanishes completely at later times (t > 1000 s). For THCC* calculations with bare ions used as basis set, the $UO_2(OH)_2 \cdot H_2O(s)$ precipitation and dissolution fronts move through the column comparable to those calculated by MCOTAC.

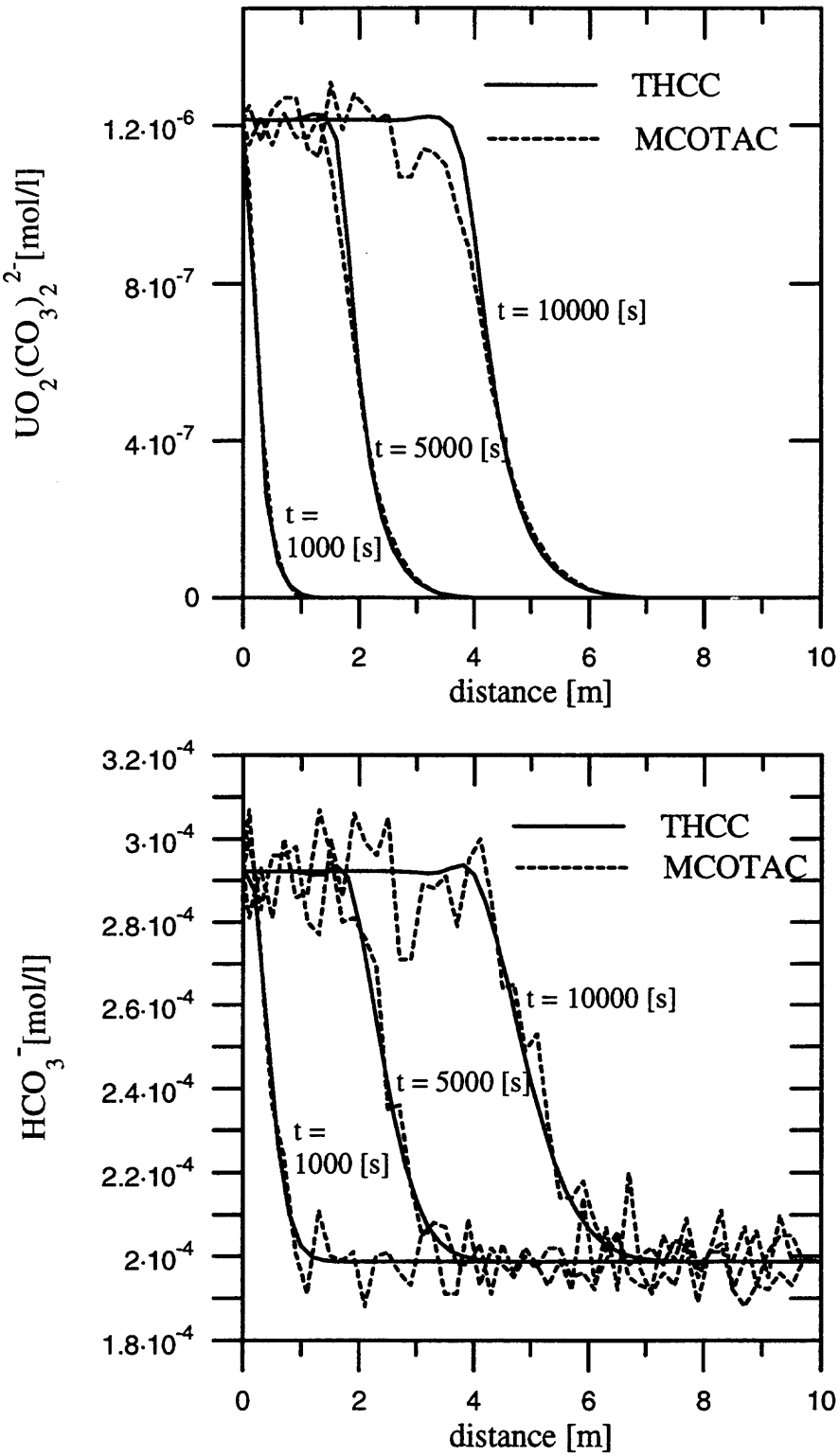

Figure B.1: Comparison of concentration profiles for the basis species $UO_2(CO_3)_2^{2-}$ and HCO_3^- calculated by THCC and MCOTAC for different migration times.

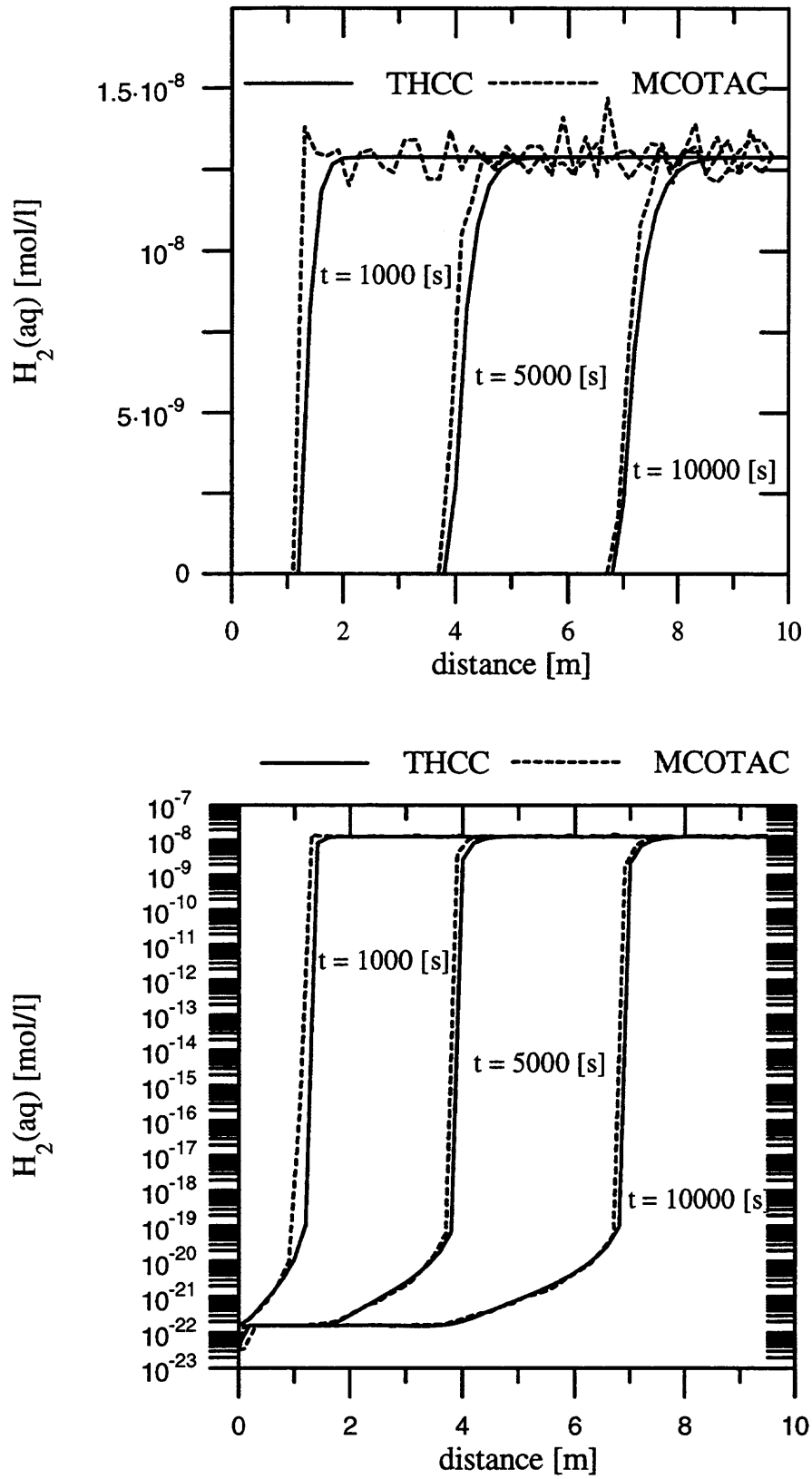

Figure B.2: Comparison of concentration profiles for the basis species $H_2(aq)$ calculated by THCC and MCOTAC for different migration times (linear-linear and log-linear scale, see footnote 6).

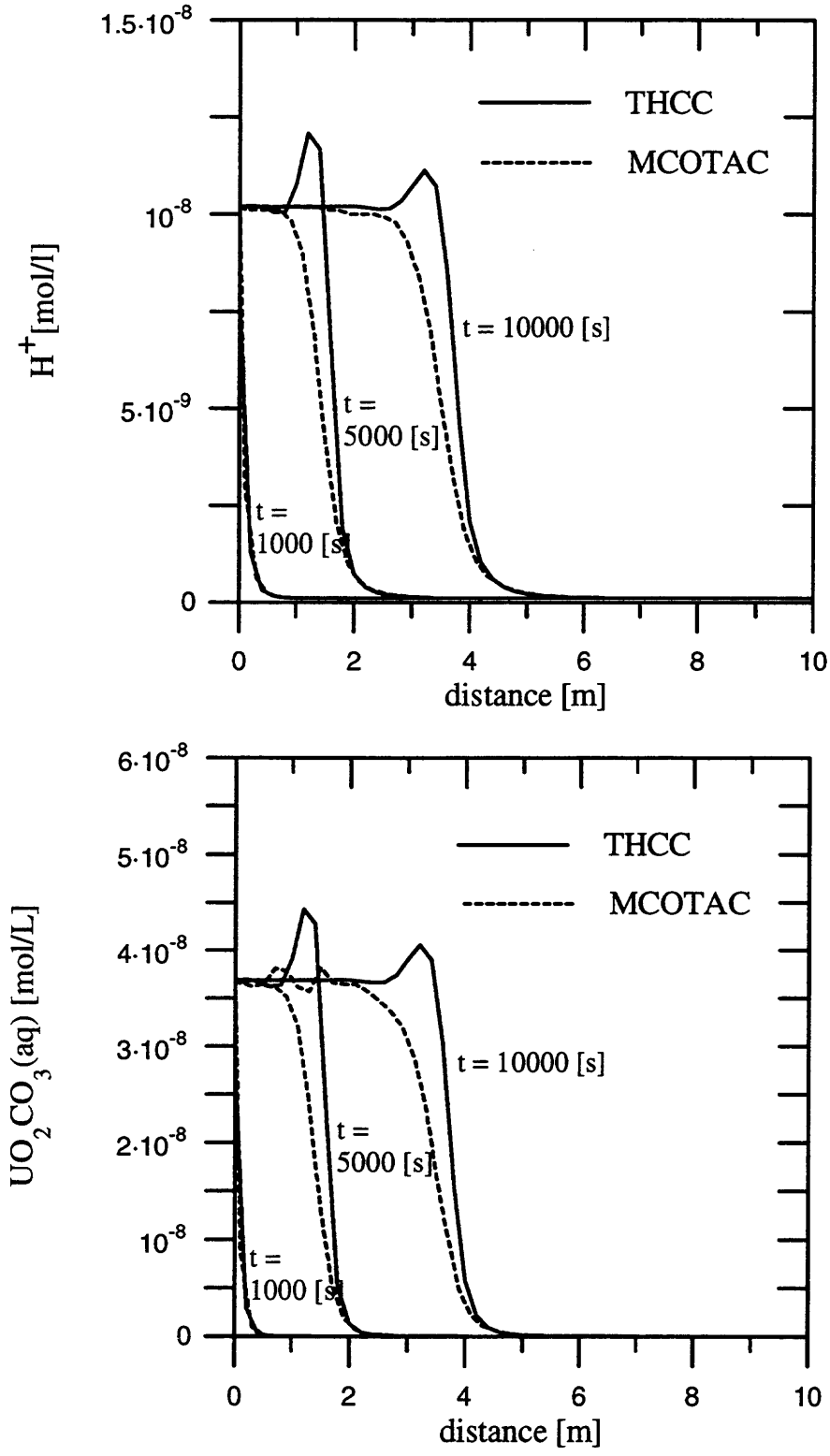

Figure B.3: Comparison of concentration profiles of complex species H^+ and $UO_2CO_3(aq)$ calculated by THCC and MCOTAC for different migration times. All profiles calculated by THCC show oscillations near the precipitation fronts.

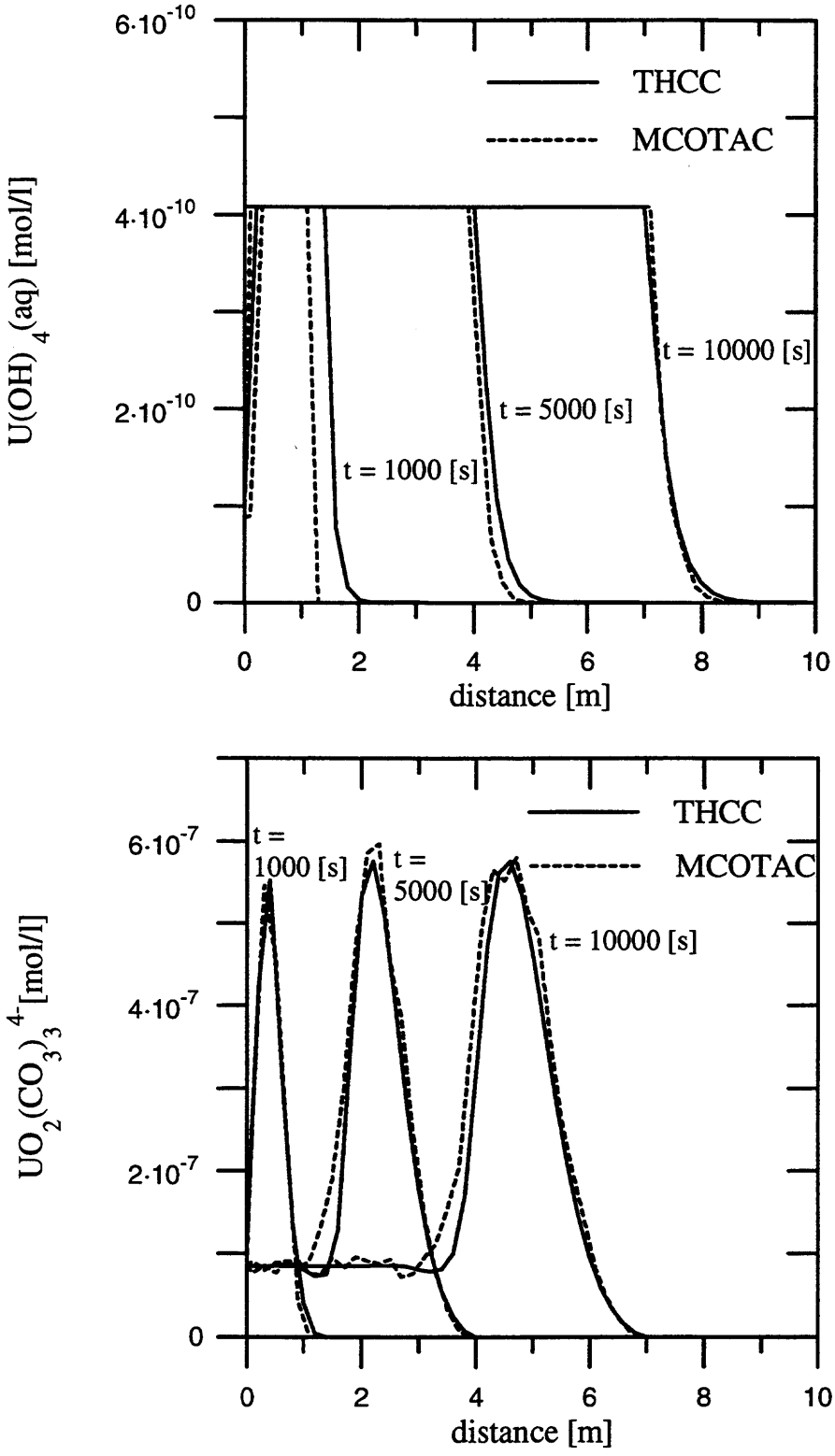

Figure B.4: Comparison of concentration profiles of complex species $UO_2(CO_3)_3^{4-}$ and $U(OH)_4(aq)$ calculated by THCC and MCOTAC for different migration times. The $UO_2(CO_3)_3^{4-}$ profiles show small oscillations to the left of the pulse profile whereas the $U(OH)_4(aq)$-profiles show no oscillations for the THCC calculation.

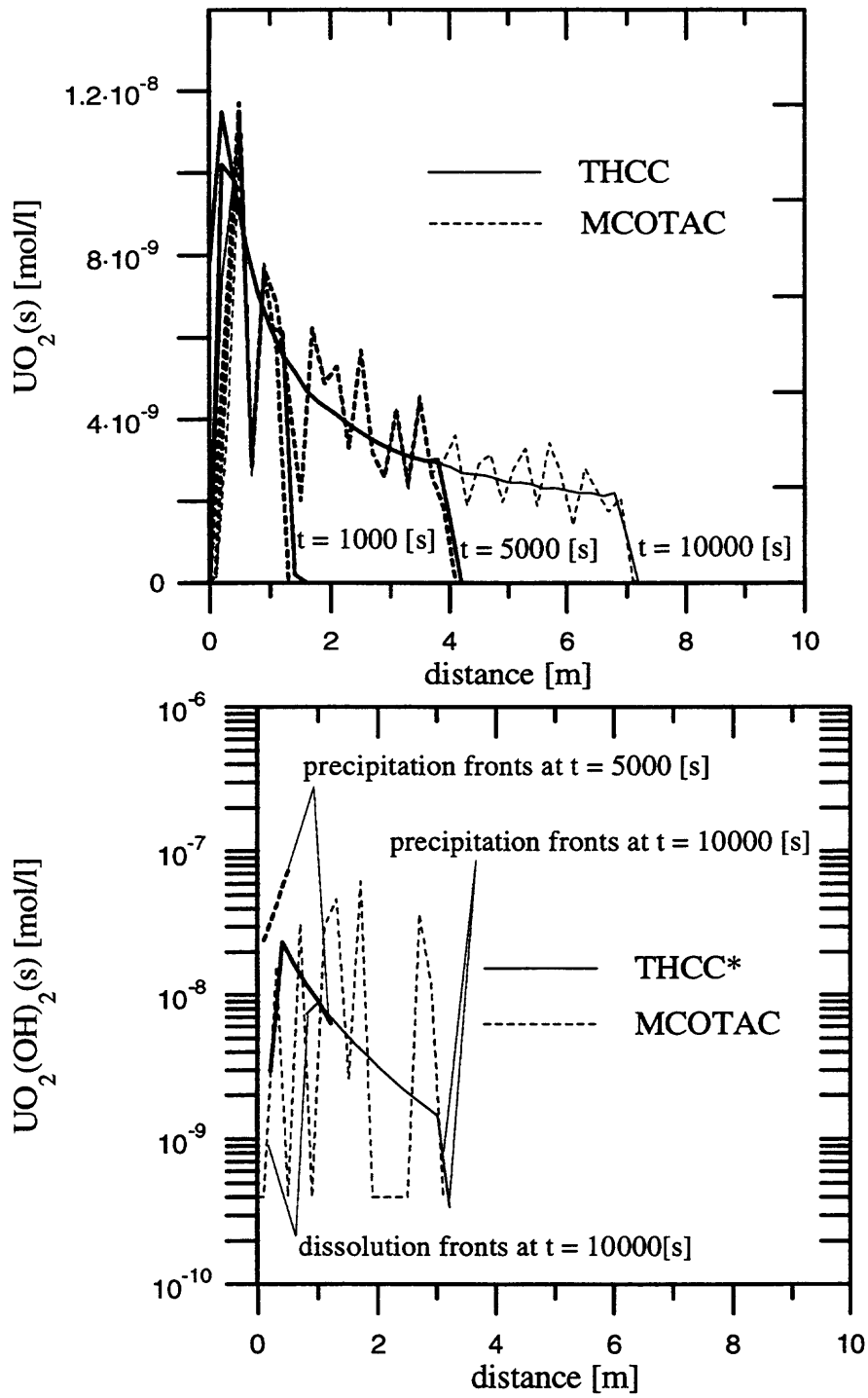

Figure B.5: *Comparison of concentration profiles of the solids $UO_2(s)$ and $UO_2(OH)_2 \cdot H_2O(s)$ calculated by THCC and MCOTAC. For THCC calculations with major ions used as basis species set the $UO_2(OH)_2 \cdot H_2O(s)$ precipitation and dissolution fronts are close together at early times (at nodes <6), and solid precipitation vanished completely at later times. For THCC* calculations with bare ions used as basis set, the $UO_2(OH)_2 \cdot H_2O(s)$ precipitation and dissolution fronts move through the column comparable to those calculated by MCOTAC.*

Appendix C: Summarised system description and calculation results related to Chapter 4.2.4 - Influence of spatial grid size

For this uranium-hydrogen system the chemical system is described by the same basis species set than used in Chapt. 4.2.1. Also the initial conditions are the same for inlet and column solution as defined in Tabs. 4.3 and 4.4. For this calculation the column length is 20 m, the grid size is 0.4 m, and the simulated migration time is 15000 s. This guarantees the same number of nodes in space, and a tracer will not migrate through the whole column during that time. For MCOTAC calculations the number of particles is also constant in comparison to former calculations. This includes a lower particle density in the 20 m long column, and related, larger fluctuations in the profiles calculated by MCOTAC.

The overall agreement in the calculated concentration profiles is the same as observed in the previous comparisons, except that the oscillations within the H^+ profiles increase strongly for THCC calculations. For the solute profiles $UO_2(CO_3)_2^{2-}$ and HCO_3^- oscillations can be observed, and already for the solids $UO_2(s)$ and $UO_2(OH)_2 \cdot H_2O(s)$ little oscillations occur in the concentration profiles at 15000 s that was not observed in previous THCC calculations.

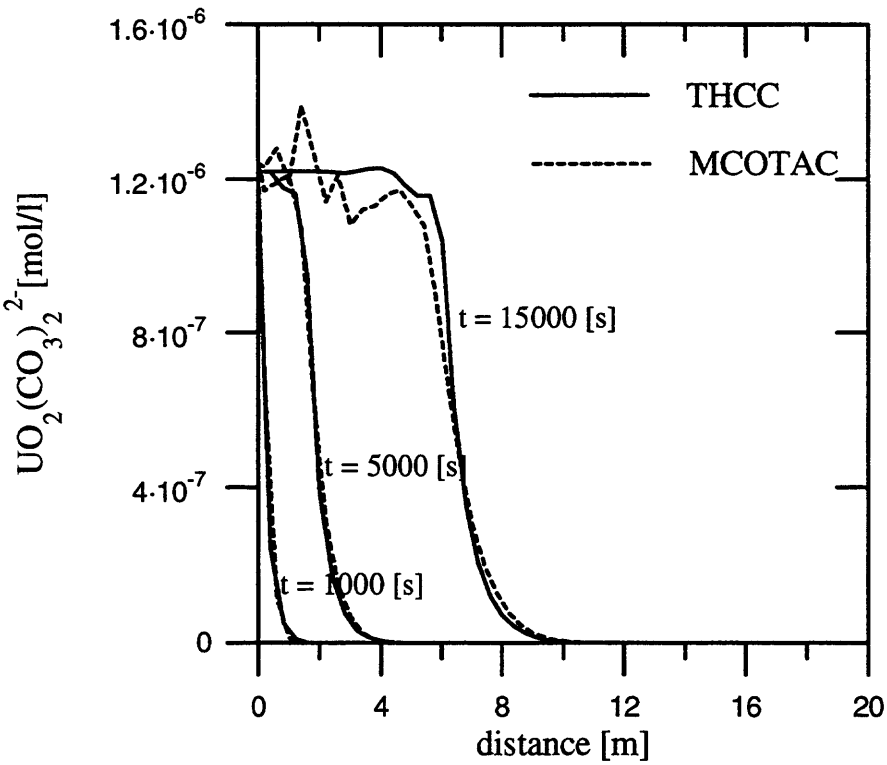

Figure C.1: Comparison of concentration profiles for the basis species $UO_2(CO_3)_2^{2-}$ calculated by THCC and MCOTAC for different migration times.

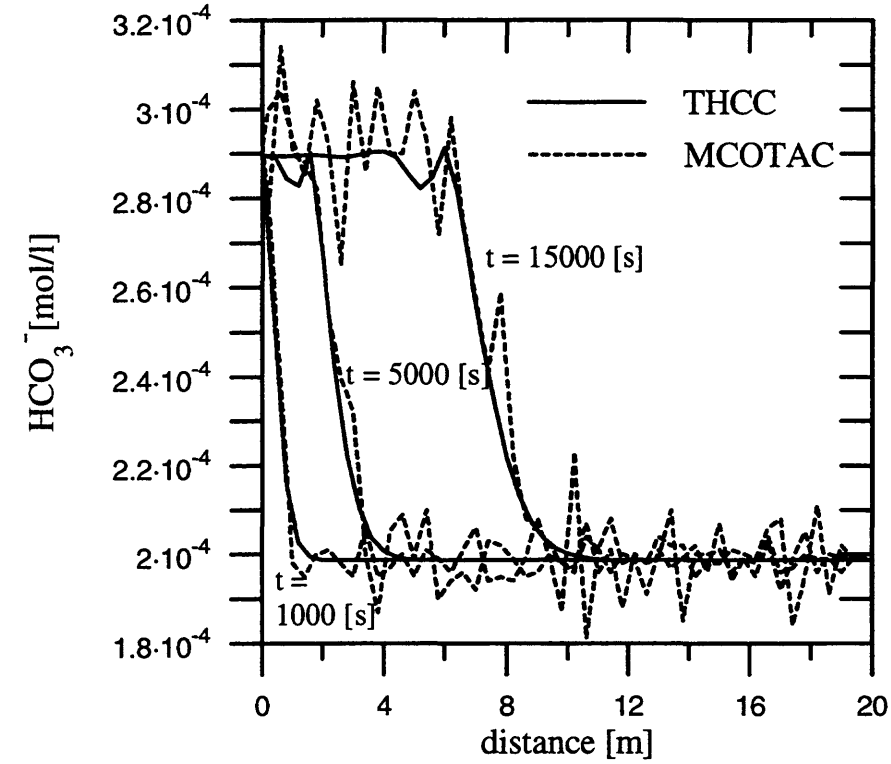

Figure C.2: Comparison of concentration profiles for the basis species HCO_3^- calculated by THCC and MCOTAC for different migration times.

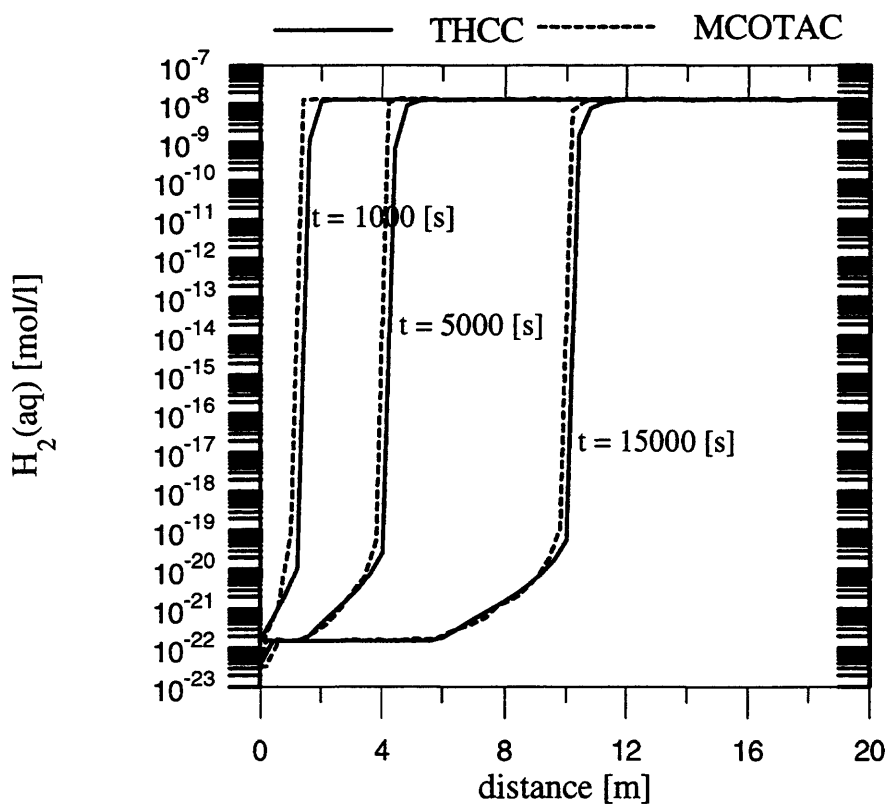

Figure C.3: Comparison of concentration profiles for the basis species $H_2(aq)$ (see footnote 6) calculated by THCC and MCOTAC.

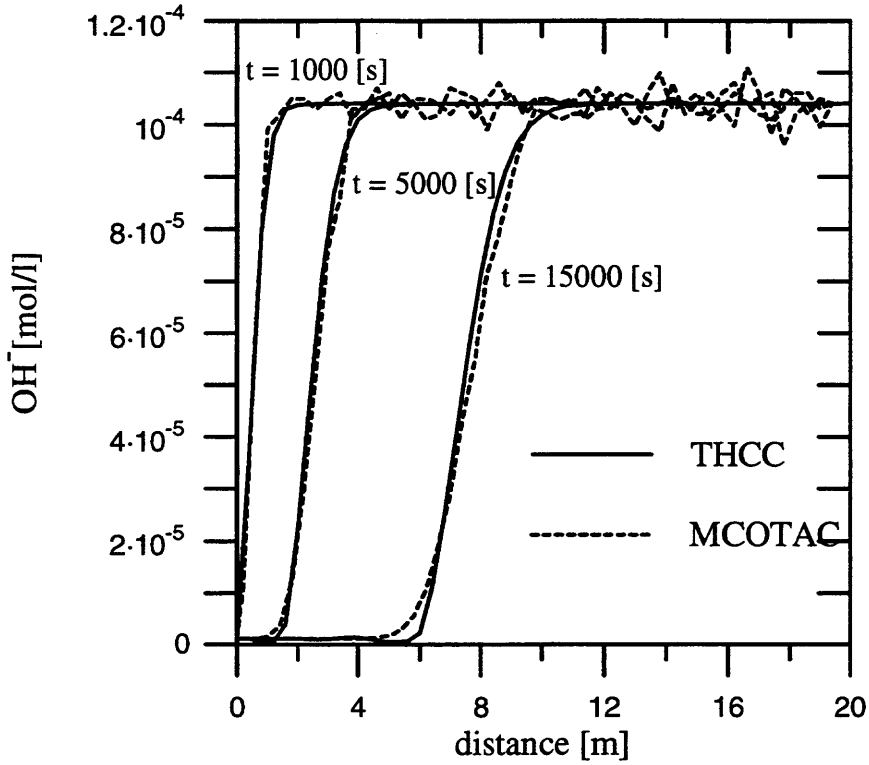

Figure C.4: Comparison of concentration profiles for the basis species OH^- calculated by THCC and MCOTAC for different migration times.

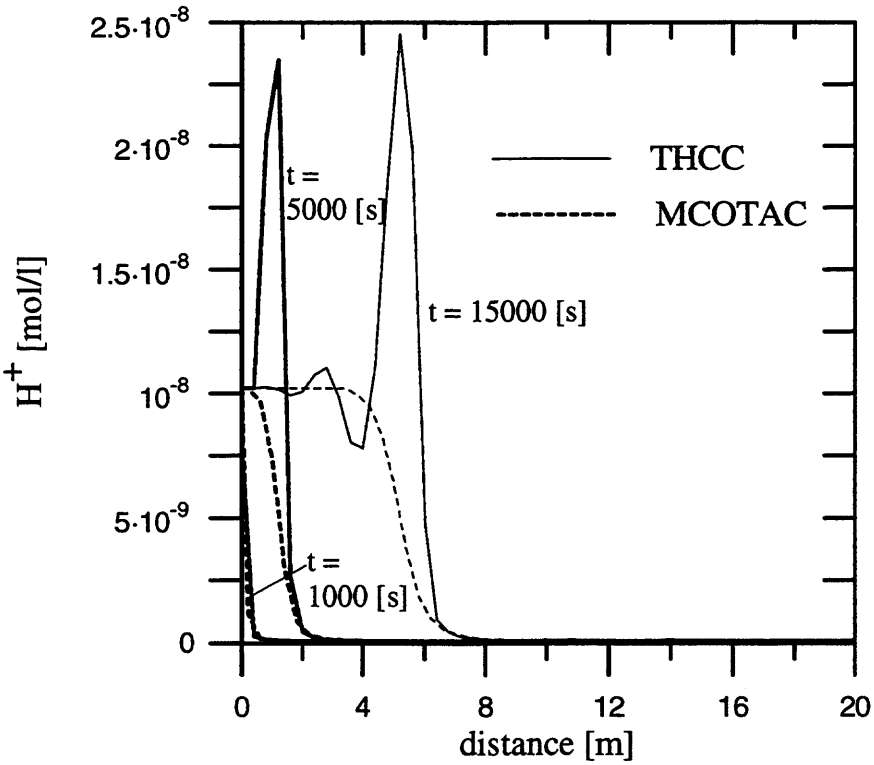

Figure C.5: Comparison of concentration profiles of the complex H^+ calculated by THCC and MCOTAC for different migration times. The H^+-profiles show the largest oscillations for a species concentration within the THCC calculation.

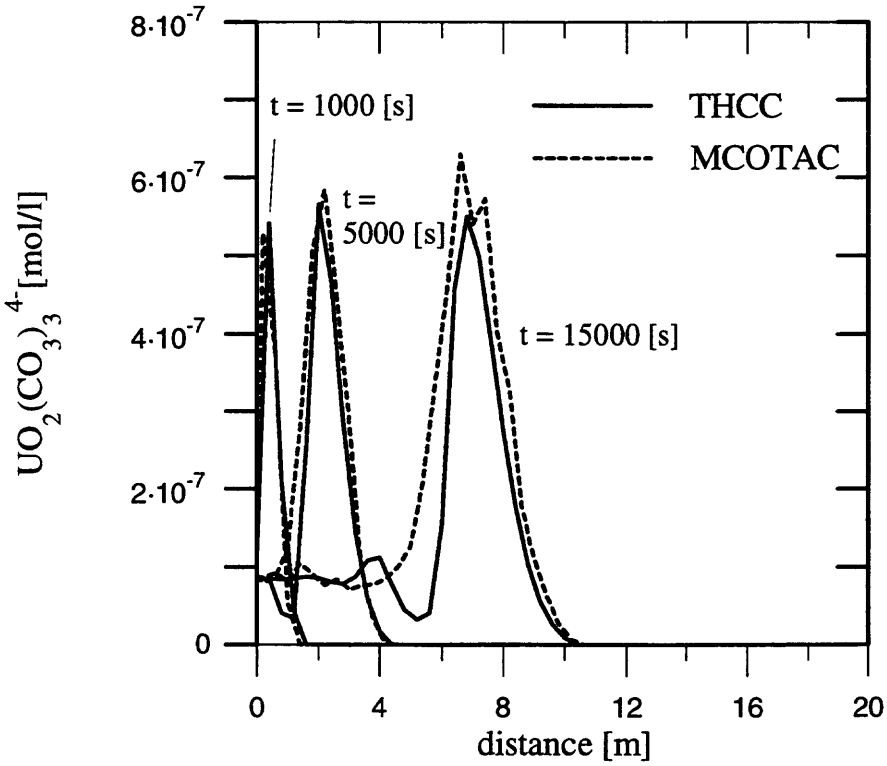

Figure C.6: Comparison of concentration profiles of the complex species $UO_2(CO_3)_3^{4-}$ calculated by THCC and MCOTAC for different migration times. The $UO_2(CO_3)_3^{4-}$ profiles showed small oscillations to the left of the pulse profile for the THCC calculation.

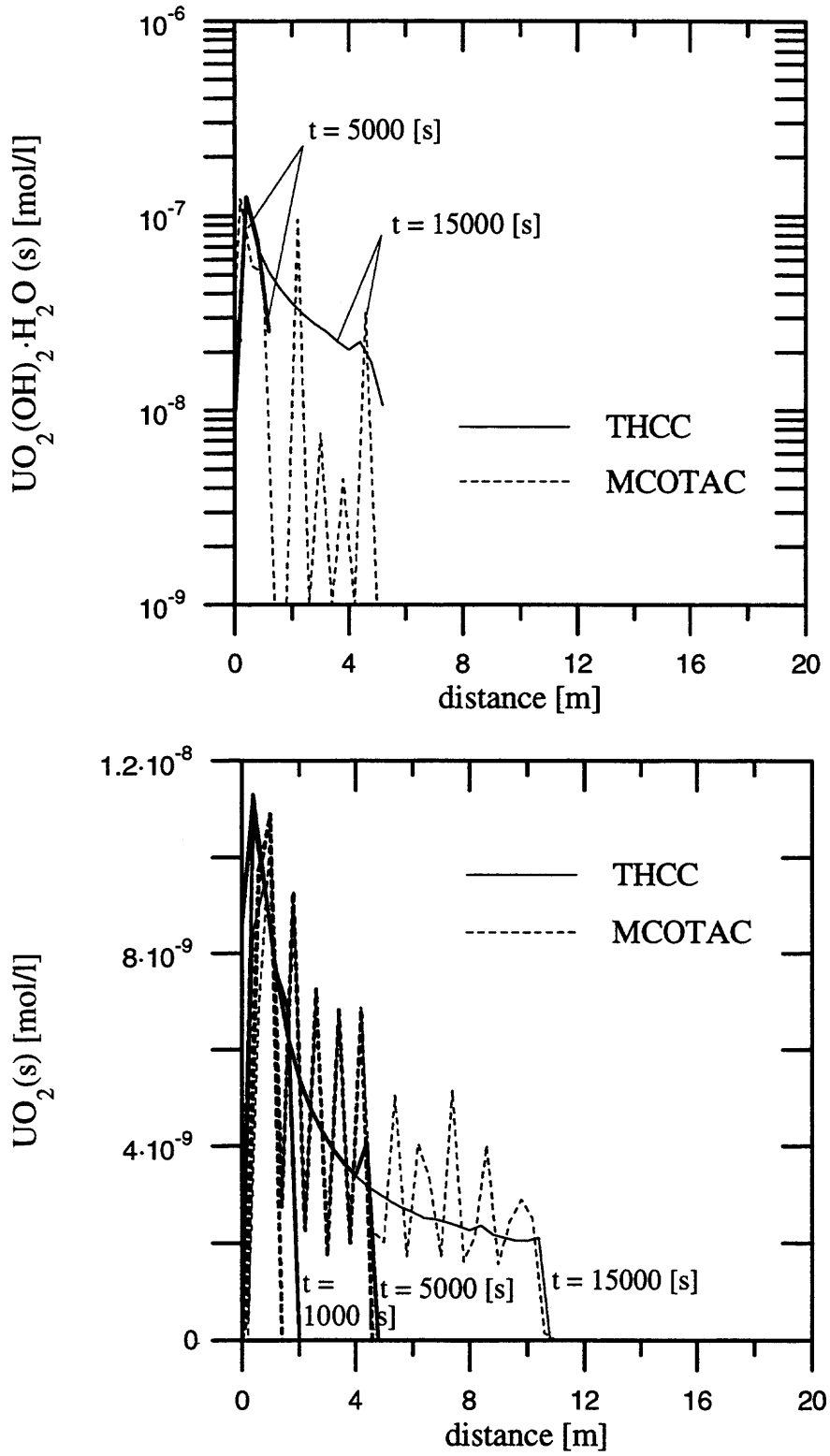

Figure C.7: Comparison of concentration profiles of the solids $UO_2(s)$ and $UO_2(OH)_2 \cdot H_2O(s)$ calculated by THCC and MCOTAC for different migration times.

Figure C.8 gives an additional impression of the overall agreement of both code applications. The precipitation fronts coincide with a general step in most species concentrations. The $UO_2(s)$ front at 9 m is not accompanied by oscillations in other concentration profiles. Hence, the $UO_2(OH)_2 \cdot H_2O(s)$ front at 4.5 m is accompanied by oscillations of some concentration profiles calculated by THCC. Small differences can be observed at low, operational concentration levels at the right side of the column where THCC calculations give a more dispersive concentration distribution than MCOTAC. This behaviour was also observed in the uranium-iron system (Fig. 3.8) and is related to the different formulation of the transport of the two codes.

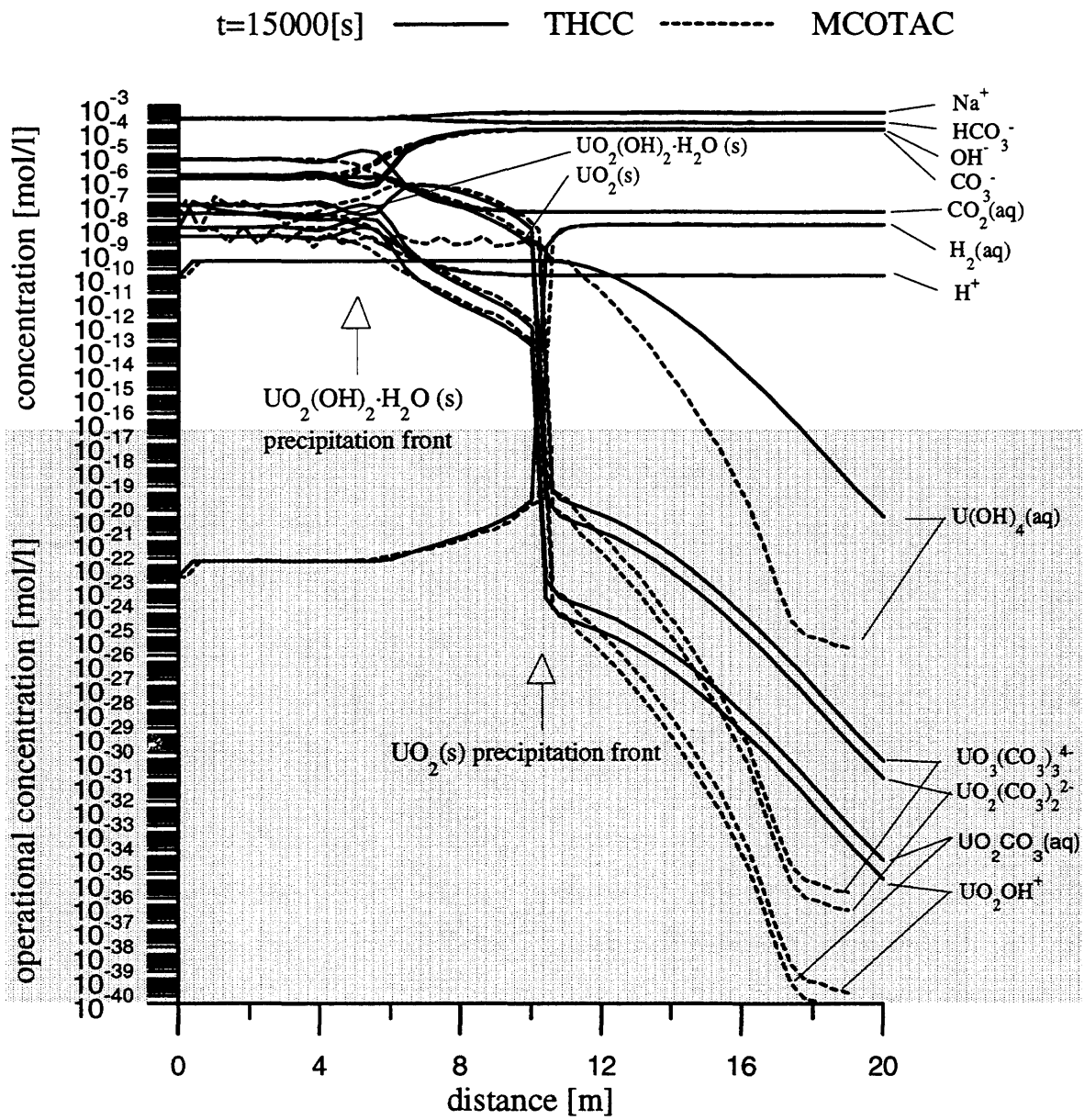

Figure C.8: Comparison of concentration profiles (see footnote 6) of all species calculated by THCC and MCOTAC. Two different precipitation fronts are located along the column: The $UO_2(s)$ front without oscillation and the $UO_2(OH)_2 \cdot H_2O(s)$ front with related oscillation of some concentration profiles of solutes.

Figure C.8 gives an additional impression of the overall agreement of both code applications. The precipitation fronts coincide with a general step in most species concentrations. The UO_2(s) front at 9 m is not accompanied by oscillations in other concentration profiles. Hence, the $UO_2(OH)_2 \cdot H_2O(s)$ front at 4.5 m is accompanied by oscillations of some concentration profiles calculated by THCC. Small differences can be observed at low, operational concentration levels at the right side of the column where THCC calculations give a more dispersive concentration distribution than MCOTAC. This behaviour was also observed in the uranium-iron system (Fig. 3.8) and is related to the different formulation of the transport of the two codes.

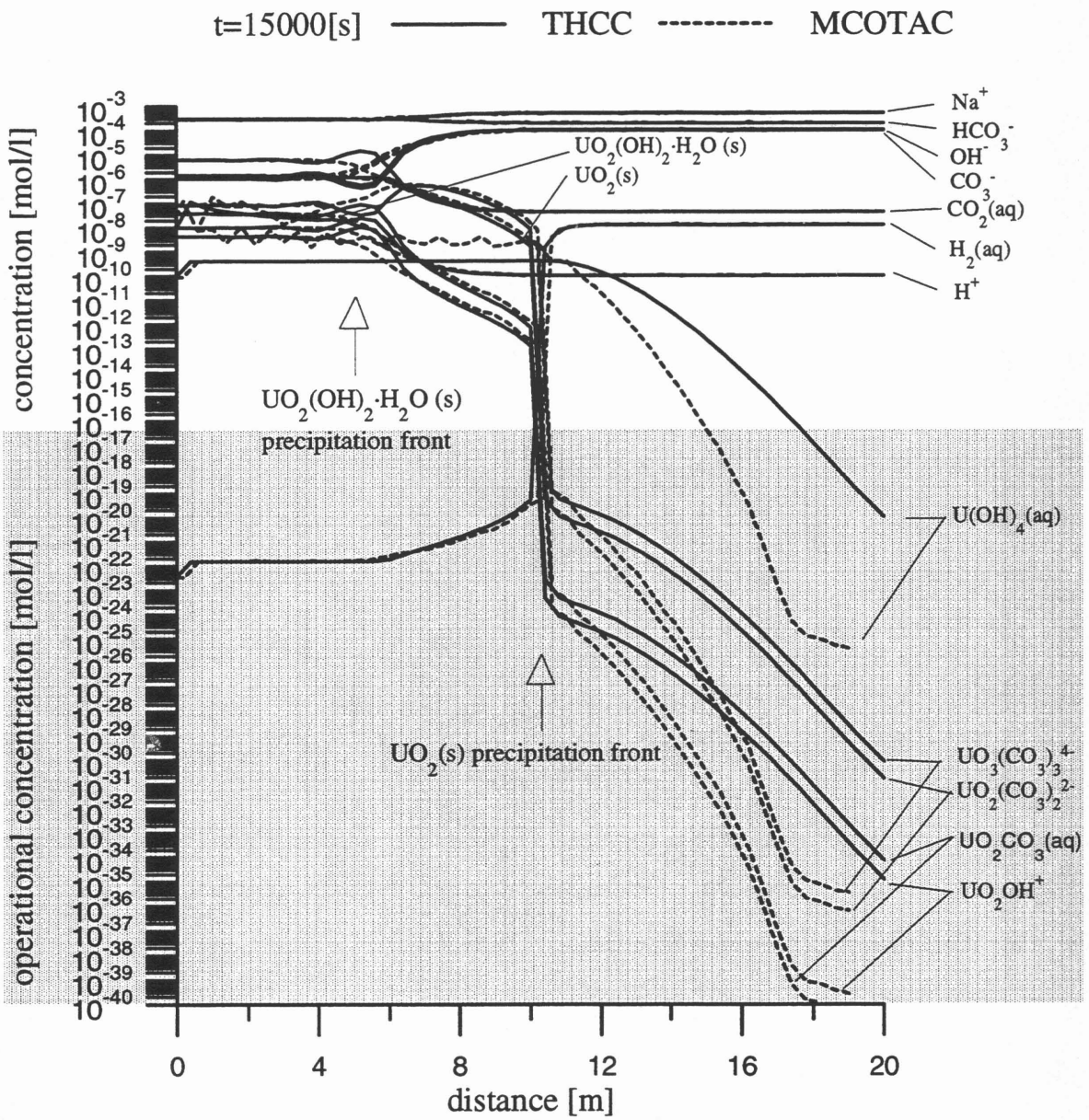

Figure C.8: Comparison of concentration profiles (see footnote 6) of all species calculated by THCC and MCOTAC. Two different precipitation fronts are located along the column: The UO_2(s) front without oscillation and the $UO_2(OH)_2 \cdot H_2O(s)$ front with related oscillation of some concentration profiles of solutes.